We are IntechOpen,
the world's leading publisher of
Open Access books
Built by scientists, for scientists

4,800

Open access books available

122,000

International authors and editors

135M

Downloads

Our authors are among the

154

Countries delivered to

TOP 1%

most cited scientists

12.2%

Contributors from top 500 universities

CLARIVATE ANALYTICS

BOOK CITATION INDEX

INDEXED

WEB OF SCIENCE™

Selection of our books indexed in the Book Citation Index
in Web of Science™ Core Collection (BKCI)

Interested in publishing with us?
Contact book.department@intechopen.com

Numbers displayed above are based on latest data collected.
For more information visit www.intechopen.com

Nanocoatings

R. Abdel-Karim and A. F. Waheed

Additional information is available at the end of the chapter

1. Introduction

Nanocoatings are one of the most important topics within the range of nanotechnology. Through nanoscale engineering of surfaces and layers, a vast range of functionalities and new physical effects can be achieved. Some application ranges of nanolayers and coatings are summarized in table 1 [1].

Surface Properties	Application Examples
Mechanical proeprties (e.g tribology, hardness, scratch resistance	Wear protection of machinery and equipment, mechanical protection of soft materials. (polymers, wod, textile, etc.), superplasticity of ceramics
Wetting properties (e.g antiadhesive, hydrophobic, hydrophibic)	Antigraffiti, Antifouling, Lotus-effect, self-cleaning surfaces.
Thermal and chemical proeprties(e.g heat resistance and insulation, corrosion resistance)	Corrosion protection for machinery and equipment, heat resistance for turbines and engines, thermal insulation equipment and building materials.
Biological properties (biocompatibility, anti-infective)	Biocompatible implants, medical tools, wound dressings.
Electronical and magnetic properties (e.g magneto resistance, dielectric)	Ultrathin dieelectrics for field effect transistors, magnetoresistive sensors and data memory.
Catalytic efficiency	Better catalytic efficiency through higher surface-to-volume.
Optical properties (e.g anti-reflection, photo-and electrochromatic)	Photo-and electrochromatic windows, antireflective screens and solar cells.

Table 1. Some applications of nanocoatings

Many synthesis techniques for production of nanostructured coatings have been developed such as sputtering, laser ablation, sol/gel technique, chemical vapour deposition, gas-conden-

sation, plasma spraying, and electrochemical deposition [1]. Chemical vapour deposition includes chemical reaction of input materials in the gas phase and deposition of the product on the surface. Physical vapour deposition (PVD) includes transforming the material into the gaseous phase and then deposition on the surface [2]. The impact of an atom or ion on a surface produces sputtering from the surface. Unlike many other vapour phase techniques there is no melting of the material. Sputtering is done at low pressure on cold substrate. In laser ablation, pulsed light from an excimer laser is focused onto a solid target in vacuum to boil off a plum of energetic atom. A substrate will receive a thin film of the target material. The sol-gel process is well adapted for ceramics and composites at room temperature [1].

The superiority of electrochemical deposition techniques in synthesizing various nanomaterials that exhibit improved compared with materials produced by conventional techniques, will be discussed. Nanocoatings can be obtained either directly on substrates or by using porous templates.

2. Electro deposition of nanomaterials

Nano crystalline materials were first reported by Gleiter [3] and due to their attractive properties. The fact that electrochemical deposition "ED", also being an atomic deposition process, can be used to synthesize nanomaterials has generated a great deal of interest in recent years. The obvious advantages of this century-old process of ED are rapidity, low cost, high purity, production of free-standing parts with complex shapes, higher deposition rates, the production of coatings on widely differing substrates. In addition, ability to produce structural features with sizes ranging from nm to μm, and ability to produce compositions unattainable by other techniques [4, 5]. This method also provides for cost-effective production of free-standing forms such as ultrathin foil, wire, sheet, and plate, as well as complex shapes.

Electro deposition parameters are bath composition, pH, temperature, over potential, bath additives, etc... Important microstructural features of the substrate include grain size, crystallographic texture, dislocation density, internal stress. Crystallization (Figure. 1) occurs either by the buildup of existing crystals or the formation of new ones. These two processes are in competition with each other and are influenced by different factors. The two key mechanisms which have been identified as the major rate-determining steps for nanocrystal formation are charge transfer at the electrode surface and surface diffusion of adions on the crystal surface [6]. With increasing inhibition, the deposit structure changes from basis oriented and reproduction type (BR) to twin transition types (TT), to field oriented type (FT), and finally to unoriented dispersion type (UD). A large number of grain refiners have been described in the literature; their effectiveness depends upon surface adsorption characteristics, compatibility with the electrolyte, temperature stability, etc. For example, saccharin, coumarin, thiorea, and HCOOH have all been successfully applied to achieve grain refinement down to the nanocrystalline range for nickel electrodeposits. The second important factor in nanocrystal formation during electro crystallization is overpotential; Grain growth is favored at low over potential and high surface diffusion rates. On the other hand, high over potential and low diffusion rates promote the formation of new nuclei [7].

2.1. Electrodeposited nanocrystalline Ni-Fe alloys

Nanostructured Ni-Fe alloys, produced by electro-deposition technique provide material with significant improved strength and good magnetic properties, without compromising the coefficient of thermal expansion (CTE). Such properties made these alloys to be used in many of the applications where conventional materials are currently used. For such applications a special attention has been made to study the physical, mechanical and chemical properties of such alloys because of the potential for performance enhancement for various applications of Ni-Fe alloys arising from the enhanced properties due to the ultra-fine grain size of these alloys [7-9].
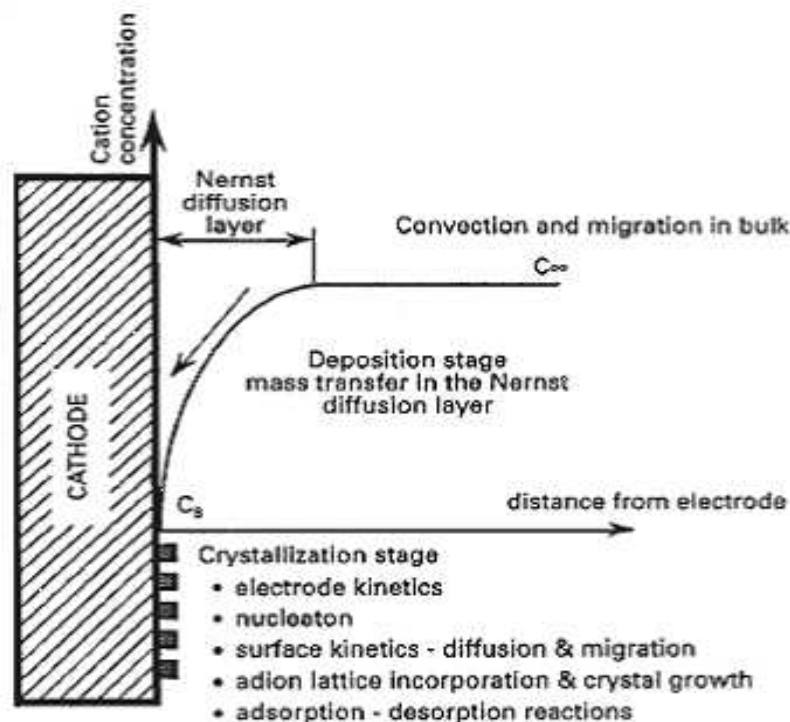

Figure 1. Two stages of electro crystallization according to Bockris et al. [6]

According to R. Abdel-Karim et al. [10], nanocrystalline Ni-Fe deposits with different composition and grain sizes were fabricated by electrodeposition. Deposits with iron contents in the range from 7 to 31% were obtained by changing the Ni^{2+}/Fe^{2+} mass ratio in the electrolyte. The deposits were found to be nanocrystalline with average grain size in the range 20–30 nm. The surface morphology was found to be dependent on Ni^{2+}/Fe^{2+} mass ratio as well as electroplating time. Figure 2 represents SEM of electrodeposited Ni base layers at longer electrode position time (100 min) as a function of Ni^{2+}/Fe^{2+} mass ratio in the electrolytic bath. From Figure 2(a), in case of Ni^{2+}/Fe^{2+} mass ratio equal to 20.7, SEM image displayed well defined nodular coarse and fine particles with no appearance of grain boundaries. This nanosized particles can be better illustrated by using higher magnification (100000x), as shown in Figure 2(b). From Figure 2(c), sample of Ni^{2+}/Fe^{2+} mass ratio equal to 13.8 displayed clusters of fine particles embedded

in elongated elliptical ones and some grain boundaries can be seen. By raising the iron content and thus decreasing the Ni^{2+}/Fe^{2+} mass ratio down to 9.8 (Figure 2(d)), the surface morphology showed rough cauliflower structure. The cauliflower morphology particle is made of coagulate particle distributed all over the surface with a flattened grains. The grains size decreased with increasing the iron content, especially in case of short time electroplating. Increasing the electroplating time had no significant effect on grain size. The microhardness of the materials followed the regular Hall-Petch relationship with a maximum value (762 Hv) when applying Ni^{2+}/Fe^{2+} mass ratio equal to 9.8.
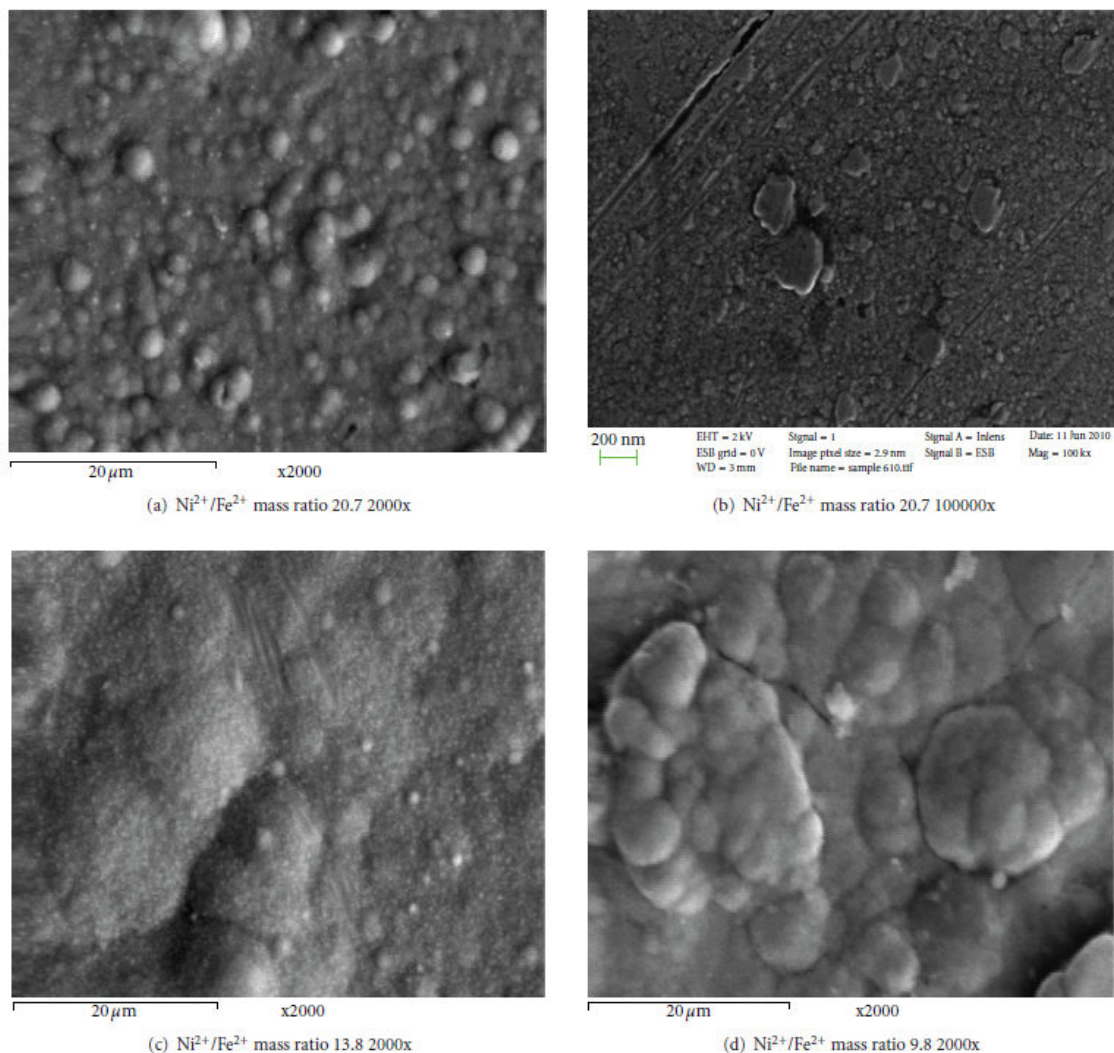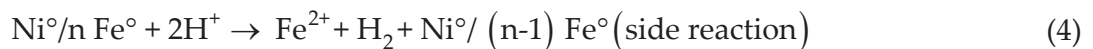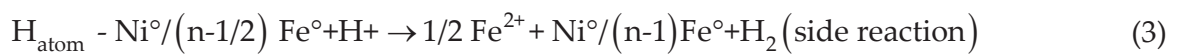

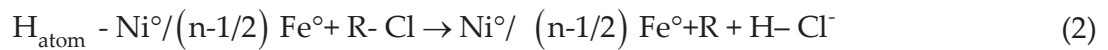**Figure 2.** SEM of electrodeposited Ni-Fe layers at current density 20 mV/cm² and deposition time 100 min. as a function of Ni^{2+}/Fe^{2+} mass ratio in the electreolyte [10].

2.2. Mechanism of electro deposition of Ni-Fe alloys

Electro deposition of Ni-Fe alloys exhibit the phenomenon of "anomalous codeposition". This term introduced by Brenner [11] is being used to describe the preferential deposition of the

less noble metal, Fe, to the more noble metal, Ni. In other words, the reduction of nickel is inhibited while the deposition of iron is enhanced when compared with their individual deposition rates. According to Afshar et al. [12], the electrode position of nickel-iron alloys is a diffusion-controlled process with typical nucleation mechanism. According to Krause et al. [13], the anomalous behavior was assumed due to precipitation of iron hydroxide on surface electrode that inhibits the nickel reduction.

$$Ni° / nFe° + H^+ \rightarrow 1/2 \ Fe^{2+} + H_{atom} - Ni°/ \ (n\text{-}1/2) \ Fe \tag{1}$$

$$H_{atom} - Ni°/(n\text{-}1/2) \ Fe° + R\text{-} Cl \rightarrow Ni°/ \ (n\text{-}1/2) \ Fe° + R + H\text{--} Cl^- \tag{2}$$

$$H_{atom} - Ni°/(n\text{-}1/2) \ Fe° + H+ \rightarrow 1/2 \ Fe^{2+} + Ni°/(n\text{-}1)Fe° + H_2 \left(side \ reaction\right) \tag{3}$$

$$Ni°/n \ Fe° + 2H^+ \rightarrow \ Fe^{2+} + H_2 + Ni°/ \ (n\text{-}1) \ Fe° \left(side \ reaction\right) \tag{4}$$

$$O_2 \left(g\right) + 2H_2O + 4e \rightarrow 4OH^- \tag{5}$$
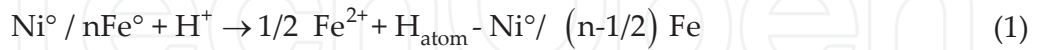
2.3. Phase formation

One of the important observations in the Ni-Fe alloys is the dependence of the crystal structure on the iron and nickel content in the deposited layers. Figure 3 shows X-ray diffraction patterns of various nanocrystalline Ni-Fe electrodeposits ranging in nickel content from 0 to 100%. Ni-Fe deposits with low nickel concentrations were found to have a body centered cubic (BCC) structure, while those with high nickel concentrations had a face-centered (FCC) structure [13]. While a mixed FCC/BCC structure was observed for nickel concentrations ranging from 10wt % to 40wt% nickel.

2.4. Properties of electrodeposited nanocrystalline Ni-Fe alloys

The first group of properties are strongly dependent on grain size. These include strength, ductility and hardness, wear resistance and coefficient of friction, electrical resistivity, coercivity, solid solubility, hydrogen solubility and diffusivity, resistance to localized corrosion and intergranular stress corrosion cracking, and thermal stability.

On the other hand, the second group of properties including bulk density, thermal expansion, Young's modulus resistance to salt spray environment, and saturation magnetization are little affected by grain size [5].
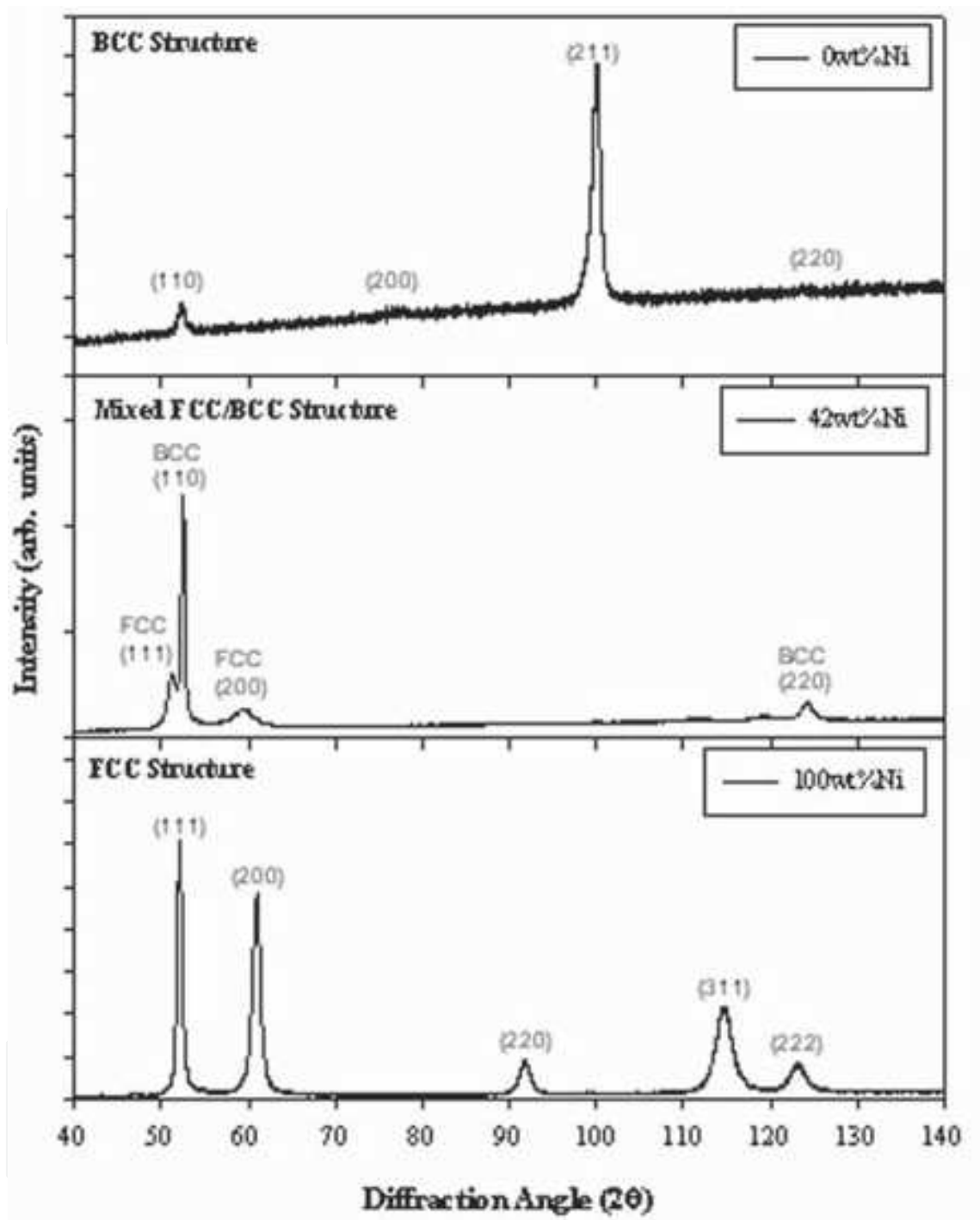
Figure 3. X-Ray diffraction patterns of electrodeposited Ni-Fe alloys with various Fe concentrations [13]

2.4.1. Mechanical properties

The plastic deformation behavior of electrodeposited nanocrystalline materials is strongly dependent on grain size. Initial increases, followed by significant decreases in hardness are observed with decreasing grain size (d) in the nanocrystal range, i.e., d ≤20 nm. The observed decreases in hardness are contrary to Hall-Petch behavior and consistent with results reported

elsewhere for nanocrystalline materials. Others have only reported a reduction in the Hall-Petch slope in the nanometer range [5].

The grain size dependence of the proof stress was found to obey the Hall-Petch relationship; however, at constant grain size, lower values were always obtained with the equiaxed geometry, are shown in Table 2. In addition to the remarkable increases in hardness, yield strength, and ultimate tensile strength with decreasing grain size, it is interesting to note that the work hardening coefficient decreases with decreasing grain size to virtually zero at a grain size of 10 nm. The ductility of the material decreases with decreasing grain size from 50% elongation to failure in tension for conventional material to 15% at 100nm grain size and about 1% at 10 nm grain size. Generally somewhat greater ductility was observed in bending. A slight recovery in ductility was observed for grain sizes less than 10 nm. Compared to conventional polycrystalline Ni, nanocrystalline Ni electrodeposits exhibited drastically reduced wear rates and lower coefficients of friction as determined in dry air pin-on-disc tests. Contrary to earlier measurements on nanocrystalline materials prepared by consolidation of precursor powder particles, nanocrystalline nickel electrodeposits do not show a significant reduction in Young's modulus [4, 14]. This result provides further support for earlier findings of Krstic et al. [15], and Zugic et al. [16], which demonstrated that the previously reported reductions in modulus with nanoprocessing were likely the result of high residual porosity.

Property	Conventional	Nano Ni, 100 nm	Nano Ni, 10 nm
Yield strength, MPa (25 ⁰C)	103	690	900
Yield strength, MPa (350 ⁰C)	--	620	--
Ultimate tensile strength, MPa (25 ⁰C)	403	1100	2000
Ultimate tensile strength, MPa (350 C)	--	760	--
Tensile elongation, % (25 ⁰C)	50	15	1
Elongation in bending, % (25 ⁰C)	--	40	--
Modulus of elasticity, GPa (25 ⁰C)	207	214	204
Vickers Hardness, Kg/mm2	140	300	650
Work hadnening coefficient	0.4	0.15	0.0
Fatigue strength, MPa (108 cycles/air/ 25 ⁰C)	241	275	--
Wear rate (dry air pin on disc, μm3/μm	1330	--	79
Coefficient of friction (dry air pin on disc)	0.9	--	0.5

Table 2. Mechanical properties of conventional and nanocrystalline Nickel

Due to Hall-Petch strengthening, nanocrystalline alloys offer significantly increased strength and hardness over conventional alloys. The table 3 summarizes tensile test data for Prem alloy (Fe-80% Ni- 4.8% Mo) and a nanocrystalline Ni-Fe alloy close to the Prem alloy in composition with average grain size between 10-15 nm. It is obvious that the yield strength, ultimate tensile strength and Vickers hardness values of the nanocrystalline Ni~20% Fe alloy significantly exceed those for the conventional Prem alloy. While the ductility represented in the elongation percentage of the conventional Prem alloy is much greater than that of the nanocrystalline

Ni~20% Fe alloy. Also figure 4 shows the Vickers hardness of nanocrystalline Ni-Fe alloys as a function of Iron content in the deposits along with the hardness values of for various conventional Ni-Fe alloys. The average hardness of the nanocrystalline Ni-Fe alloys is approximately 4 to 7 times higher than that of the conventional alloys as seen in table 3 and Figure 4. Besides, Figure 4 shows that there is a moderate decrease in the hardness with increasing the Iron content in the FCC range and a significant increase with Fe- content in the BCC range and a minimum hardness at the FCC-BCC transition [14].

Material	Yield strength 0.2% Offset MPa	Ultimate tensile strength	% Elongation	Vickers Hardness (VHN)
Nano-Ni-20% Fe	1785	2250	3-4%	550-600
Conv Premalloy	207	550	30%	100

Table 3. Mechanical properties of nanocrystalline Ni-20%Fe and conventional Prem alloy
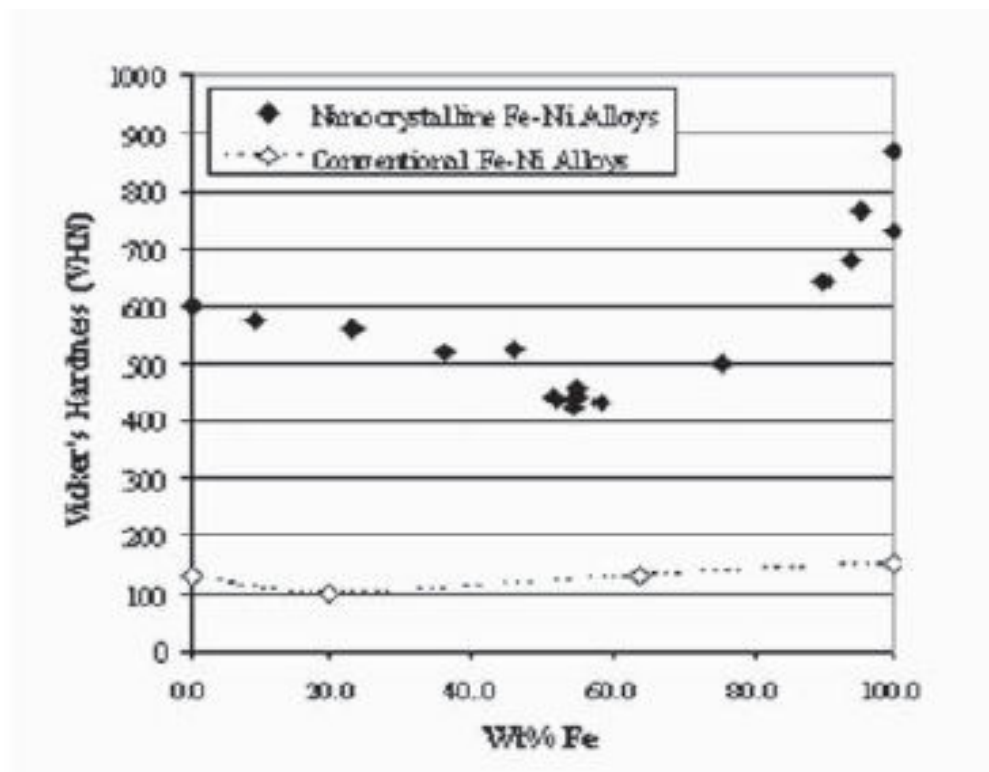

Figure 4. Vickers hardness as a function of iron content for various conventional and nanocrystalline Ni-Fe alloys [14].

2.4.2. Corrosion properties

In general, the corrosion resistance of nanocrystalline materials in aqueous solutions is of great importance in assessing a wide range of applications. To date, research in this area is still scarce and relatively few studies have addressed this issue. For the case of the corrosion behavior of

nanocrystalline materials produced by crystallization of amorphous precursor materials; both beneficial and detrimental effects of the nanostructure formation on the corrosion performance were observed. The conflicting results are, to a large extent, due to the poorly characterized microstructures of the crystallized amorphous materials. On the other hand, for nanostructured materials produced by electro deposition, considerable advances in the understanding of microstructure on the corrosion properties have been made in recent years [18].

In previous studies, potentiodynamic and potentiostatic polarizations in de-aerated 2N H_2SO_4 (pH = 0) were conducted on bulk (2 cm^2 coupons, 0.2 mm thick) nanocrystalline pure Ni at grain sizes of 32, 50, and 500 nanometers and compared with polycrystalline pure Ni (grain size of 100 μm). Figure 5 shows the potentiodynamic anodic polarization curves of these specimens. The nanocrystalline specimens exhibit the same active-passive-transpassive behavior typical of conventional Ni. However; differences are evident in the passive current density and the open circuit potential. The nanocrystalline specimens show a higher current density in the passive region resulting in higher corrosion rates. These higher current densities were attributed to the higher grain boundary and triple junction content in the nanocrystalline specimens, which provide sites for electrochemical activity. However, this difference in current density diminishes at higher potentials (1100 mV SCE) at which the overall dissolution rate overcomes the structure-controlled dissolution rate observed at lower potentials [19].
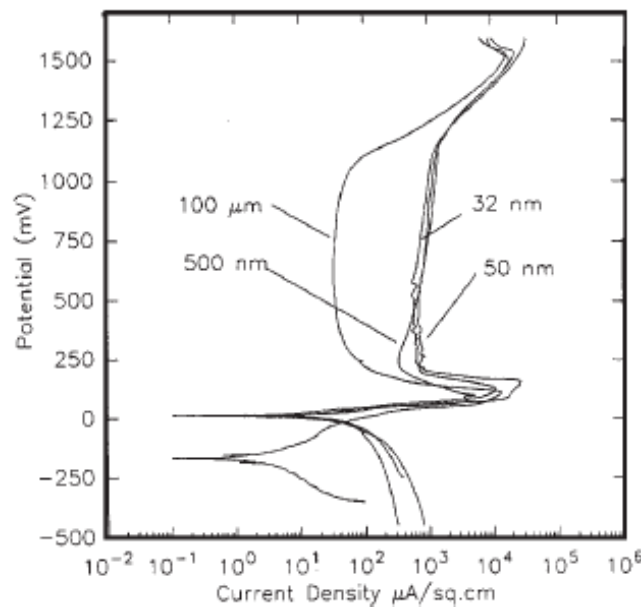

Figure 5. Potentiodynamic polarization curves for nanocrystalline and polycrystalline Ni in 2N H_2SO_4 at ambient temperature [19].

Figure 6 shows scanning electron micrographs of nickel with a) 32 nm and b) 100 μm grain size, held potentiostatically at 1200 mV (SCE) in $2NH_2SO_4$ for 2000 seconds. Both specimens exhibit extensive corrosion but the nanocrystalline Ni is more uniformly corroded while the specimen with 100 μm grain size shows extensive localized attack along the grain boundaries and triple junctions. X-ray photoelectron spectroscopy of the specimens polarized in the
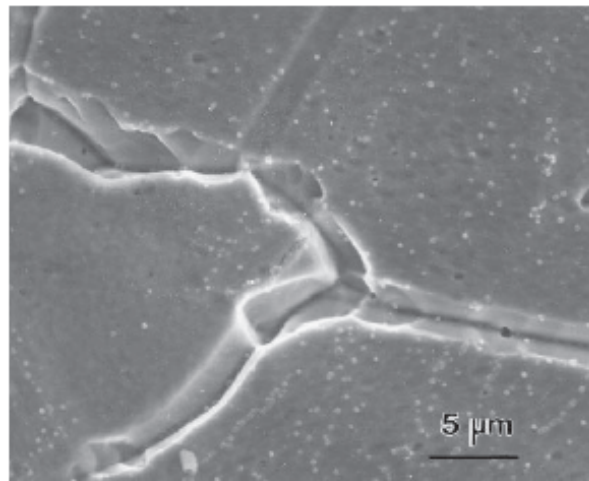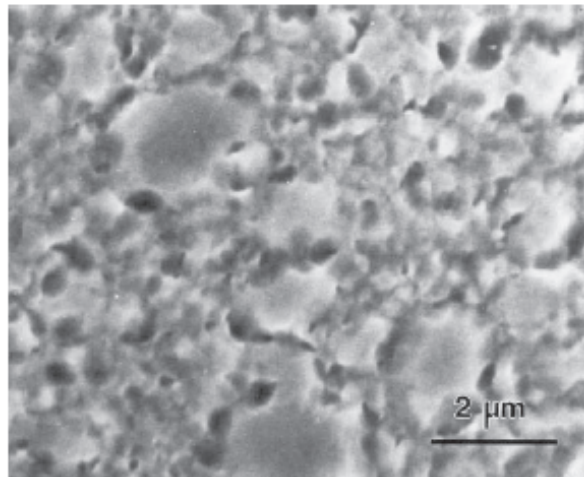
Figure 6. SEM micrographs of Ni with (a) 100 μm and (b) 32 nm grain size held potentiostatically at 1200 mV (SCE) in 2N H_2SO_4 for 2000 seconds [19].

passive region proved that the passive film formed on the nanostructured specimen is more defective than that formed on the polycrystalline specimen, while the thickness of the passive layer was the same on both specimens. This higher defective film on the nanocrystalline specimen allows for a more uniform breakdown of the passive film, which in turn leads to a more uniform corrosion. In contrast, in coarse-grained Ni the breakdown of the passive film occurs first at the grain boundaries and triple junctions rather than the crystal surface, leading to preferential attack at these defects [19].

The corrosion behavior of nanocrystalline Ni was also studied in 30 wt% KOH solution and pH neutral solution containing 3 wt% sodium chloride. The results were similar to the corrosion behavior observed in sulfuric acid. The general corrosion was somewhat enhanced

compared to conventional polycrystalline Ni; however, the nanostructured materials were much more immune to localized attack which often can lead to catastrophic failures.

Comparing bulk nickel to nanocrystalline nickel, it is found that the bulk nickel was more resistant to anodic dissolution once the free corrosion potential had established. This interesting result because it indicates that once free corrosion conditions have been established, the surface of nanocrystalline nickel is more susceptible to corrosion than bulk nickel. It is known that the primary passivation potential of binary Ni-Fe alloys generally increase with increasing nickel concentration, comparatively little study has been conducted on the corrosion behavior of these alloys in nanocrystalline form. A study on the pitting behavior of nanocrystalline Ni-18% Fe found that it was more susceptible to pitting corrosion after significant grain growth had occurred during annealing [20]. Another study of the corrosion resistance of electrodeposited nanocrystalline Ni-W and Ni-Fe-W alloys reported poor corrosion resistance for the ternary alloy because of preferential dissolution of Fe. While alloy concentration effects on the corrosion rate of electrodeposited nanocrystalline Ni-Fe alloys remain to be clearly established, as the Iron content in the alloy is increased, the corrosion rate is increased simultaneously [21].

2.4.3. Electric and magnetic properties

As the average grain size in the nanocrystalline materials is reduced to the extent that the domain wall thickness is comparable to the grain size, the coercively is found to dramatically decrease while for the permeability of such alloys will increase. Another consequence of the ultra-fine grain size of nanocrystalline materials is an increase in the electrical sensitivity over the polycrystalline materials due to the high volume of grain boundaries. The electrical resistivity of electrodeposited nanocrystalline Ni-Fe alloys has been found to increase considerably as the grain size decreases to less than 100 nm [5, 22, 23].

2.4.4. Coefficient of thermal expansion

The grain size reduction to about 10nm in fully dense electrodeposited material has no major effect on the thermal expansion. Comparing between the coefficients of thermal expansion of nanocrystalline Fe-43wt% Ni to that of Ni-Fe conventional alloys it was found that both have similar values [18].

2.5. Applications of Ni-Fe alloys

Nickel-iron alloys are of great commercial interest as a result of their low thermal expansion and soft magnetic properties.

2.5.1. Low thermal expansion applications of Ni-Fe alloys

The nanocrystalline Ni-Fe alloys are used in the integrated circuit packaging and shadow masks for cathode ray tubes where they require a low coefficient of thermal expansion and also additional strength would be beneficial. For the integrated circuit packaging materials, they require materials with thermal coefficient matched to those of silicon to prevent the

formation of cracks, de-lamination and/or de-bonding of the different materials during thermal cycles to which the components are exposed [14].

In the color cathode ray tube televisions and computer monitors, the shadow mask is a perforated metal sheet which the electrons from the electron gun must pass through before reaching the phosphor screen. Its role is to ensure that the electron beam hits only the correct colored dots and does not illuminate more than the one that was intended. Only 20% of the electrons pass through the shadow mask, and the other 80% are being absorbed by the mask which leads to an increase in the temperature of the mask. The resulting thermal expansion can disturb the alignment between the apertures and the phosphor triads, leading to a distorted image. This effect is known as "doming [14].

The main advantages of using electrodeposited nanocrystalline over conventional Ni-Fe alloys -for the use in integrated circuit packaging or shadow masks- for cathode ray tubes include:

- Single step process to produce foils ranging in thickness from 150μm to 500μm;

- High mechanical strength and hardness (> 450VHN);

- Isotropic properties due to fine equiaxed grain structure;

- Improved chemical machining performance;

- Finer pitch possible due to a decrease in grain size and higher strength;

- High etch rates due to increased grain boundary volume fraction [14].

2.5.2. Magnetic applications of Ni-Fe alloys

For soft magnetic applications, such as electromagnetic shielding, transformers materials, read-write heads, and high efficiency motors, magnetic materials- that exhibit small hysteresis losses per cycle- are required. More specifically, materials that have high permeability, low coercivity, high saturation and remnant magnetization, high electrical resistivity (to minimize losses due to eddy current formation [23-25]

3. Nanocrystalline Nickel-Molybdnum alloys

Nanostructured Ni-Mo alloys functionalized with acrylic acid (AA) and dispersed in paint have shown a satisfactory performance as corrosion inhibitors which led them to be used as anticorrosive paints for petroleum industry applications [26]. Recently, few researches have been conducted to investigate the effectiveness of nanocrystalline Ni-Mo alloys as catalysts for steam reforming of hydrocarbons, such as T. Huang et al.[27] Ni-Mo bimetallic catalyst of 20.5 nm crystallite size showed high activity, superior stability and the lowest carbon deposition rate (0.00073 gc.gcat^{-1}.h^{-1}) in 600-h time on steam.

Moreover, owing to the nanocrystalline state of Ni-Mo alloys, a large number of active sites are provided which make these alloys perfect candidates as catalysts for hydrogen production

from water electrolysis [28]. Nanocrystalline Ni-Mo alloys have been processed by different techniques such as RF magnetron sputtering, mechanical alloying and electrodeposition techniques. H. Jin-Zhao et al. [29] reported that nanocrystalline Ni-Mo alloys prepared by RF magnetron sputtering technique to be promising electrodes for hydrogen evolution reactions. While P. Kedzierzawski et al. [30] were able to produce successfully nanocrystalline Ni-Mo alloys by mechanical alloying method, as well as indicating the positive contribution of the large surface area in increasing the catalytic effect as electrodes for hydrogen production and decrease of the exchange current density.

Furthermore, several attempts have been made in order to produce nanostructured Ni-Mo alloys by electro deposition technique to be used as cathodes for hydrogen production from water electrolysis. This is because electro deposition is considered to be cheaper than other production techniques -being mentioned previously- from the aspect of initial capital investment and running costs [31, 32]. While it also require minor modifications to existing conventional plating lines to be able to produce nanocrystalline films or stand free objects, in addition to that scaling up is relatively easy and high production rates can also be achieved [33].

Ni-Mo deposits have been well known for their use as cathodes for hydrogen production from water by electrolysis as well as catalysts for hydrogen production by steam reforming of hydrocarbons [7]. Arul Raj and Venkatesan [34] showed an increased electrocatalytic effect of Ni-Mo electrodeposited alloys for the hydrogen evolution reaction than that showed by nickel and other nickel-based binary alloys such as Ni-Co, Ni-W, Ni-Fe, and Ni-Cr. In addition, Ni-Mo alloys are considered as highly corrosion resistant due to the good corrosion protection characteristics of molybdenum in non oxidizing solutions of hydrochloric, phosphoric, and hydrofluoric acid at most concentrations and temperatures and in boiling sulfuric acid up to about 60% concentration [35]. The nickel-molybdenum alloys normally containing 26–35wt% Mo are among the few metallic materials that are resistant to corrosion by hydrochloric acid at all concentrations and temperatures [36]. Electro deposition is one of the most promising techniques for producing nanostructure materials owing to its relative low cost compared to the other methods. Electro deposition produces nanocrystalline materials when the deposition parameters (e.g., plating bath composition, pH, temperature, current density, etc.) are optimized such that electrocrystallization results in massive nucleation and reduced grain growth [37, 38]. Due to better anticorrosive in several aggressive environments, mechanical and thermal stability characteristics of Ni-Mo alloys, the electro deposition of these alloys plays an important role. It is an example of the induced codeposition mechanism [39].

According to J. Halim et al [40], Ni-Mo nanocrystalline deposits (7–43 nm) with a nodular morphology (Figure 7) were prepared by electro deposition using direct current from citrate-ammonia solutions. They exhibited a single Ni-Mo solid solution phase. Increasing the applied current density led to a decrease of the molybdenum content in the deposited alloys, increase in crystallite size, and increase of the surface roughness. The highest microhardness value (285 Hv) corresponded to nanodeposits with 23% Mo. The highest corrosion resistance accompanied by relatively high hardness was detected for electrodeposits containing 15% Mo. Mo content values between 11 and 15% are recommended for obtaining better electrocatalytic activity for Hydrogen evolution reaction "HER" with the lowest cathodic Tafel's constant.
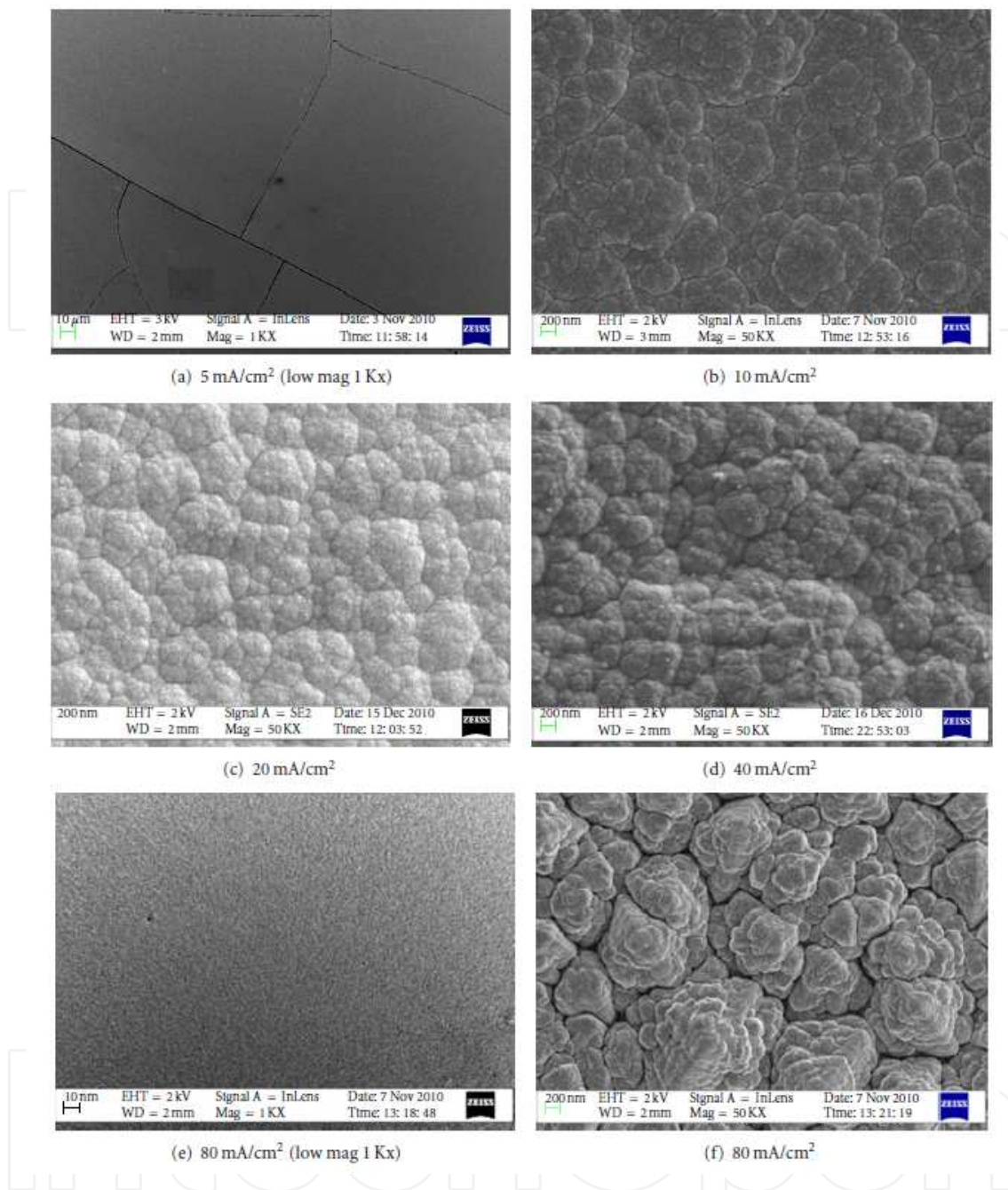
Figure 7. SEM micrograph of Ni-Mo nanocrystalline electrodeposits [40].

3.1. Mechanism of Ni-Mo electro deposition

Ni-Mo electrodeposited alloys are considered as an example of the induced codeposition mechanism. Several hypotheses have been proposed and many investigations have been carried out to describe the Ni-Mo electro deposition mechanism. According to Chassaing et al. [39], the formation of Ni-Mo electrodeposited alloy has been explained in the following steps:

1.   Reduction of molybdate to Mo (IV) oxide by Ni (II) species forming MoO_2Ni_4.

2.   Reduction of the mixed oxide (MoO_2Ni_4) forming Ni-Mo alloy.

Whereas, Podlaha and Landolt [41, 42], have proposed a model based on the adsorption and catalytic reduction of molybdate species using a bath containing citrate species. This model assumes that [Ni (II)HCit]⁻ catalyze molybdate reduction forming a surface-adsorbed inter-mediate, $[Ni(II)HCit-MoO_2]_{ads}$. The deposition of Mo, as indicated by this model, is only possible when Ni (II) ions are present, while nickel ions reduction following an independent path.

Generally, in a nickel-rich citrate electrolyte molybdenum deposition is mass-transport limited. Therefore, the Ni-Mo alloy composition is strongly influenced by the electrode rotation rate. While in a molybdenum-rich electrolyte, the rate of molybdenum deposition is limited by the flux of nickel ion. The alloy composition in this case is independent of hydrodynamic effects [41].

Electro deposition parameters have a large influence on the compostion of Ni-Mo alloys, the plating current density is one of the important deposition parameters affecting the composition of Ni-Mo alloys, and it has been investigated by many researches through different plating bathes that the molybdenum content decreases as the plating current density increases E. Chassaing et al. [39], reported the decrease of molybdenum content from 30 to about 10 wt% by increasing the current density from 10 to 150 mA/cm² as shown in the Figure 8 [42]. The same conclusion has been reached in the case of Ni-Mo alloys deposited from pyrophosphate baths as indicated by M. Donten et al. [31] that Mo content ranges from 55 to 35 wt% for a plating current density from 15 to 50 mA/cm².

As for the relationship between the Mo content in the citrate bath and that in the depos-it, the molybdenum content in the deposit increases as the metal percentage of molybde-num in the bath increases [40]. The increase in the content of sodium citrate in the bath resulted in an increase of the molybdenum content of the deposit. Moreover, the molybde-num content in the deposit showed an increased as the pH increases till about pH = 9 and then decreased.

3.2. Phase formation of nanocrystalline Ni-Mo alloys

Most of the electrodeposited Ni-Mo alloys are composed of a single phase and are mainly semi amorphous. It was found by XRD analysis that the Ni-Mo alloys electrodeposited from a citrate bath (ph 8.5-9.5) contain Ni-Mo solid solution.

With diffraction peaks being sharp at the lower content of Mo (12wt%) and wide at the high concentration of Mo (30wt%) indicating that the alloys are tending to be more amorphous as the molybdenum content increases as shown in Figure 9 [42]. A similar conclusion was made by the XRD analysis of the Ni-Mo alloys electrodeposited from pyrophosphate-ammonium-chloride bath (pH 8.5) [31].
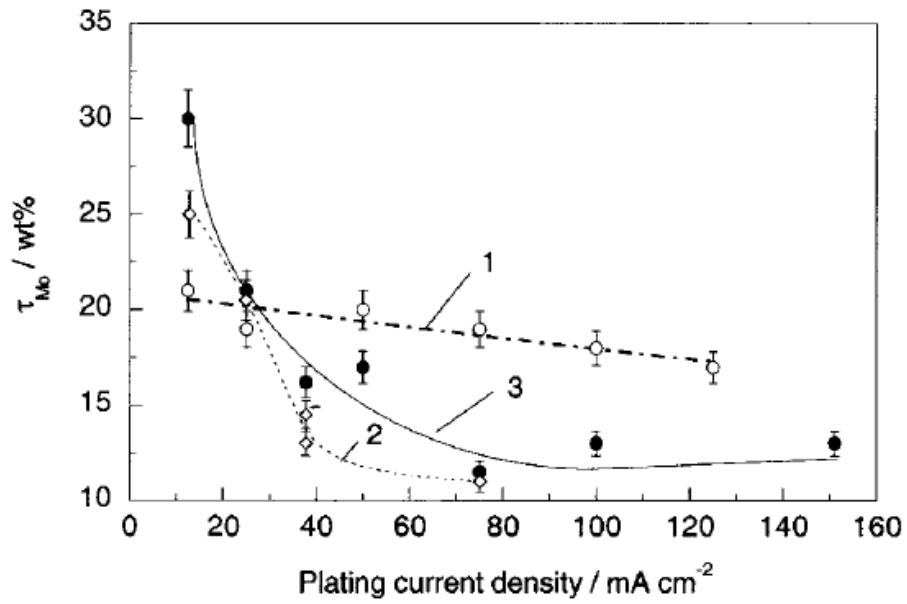
Figure 8. Molybdenum content as a function of the applied current density. Curve 1: 0.02 M Na_2MoO_4, pH 8.5; Curve 2: 0.02 M Na_2MoO_4, pH 9.5; Curve 3: 0.03M Na_2MoO_4 pH 9.5 [42].
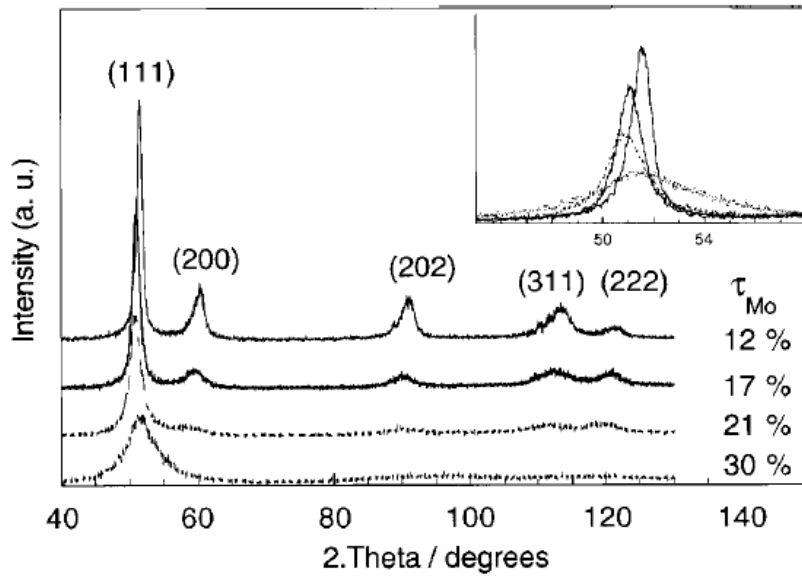

Figure 9. XRD patterns for Ni–Mo layers deposited from solution containing 0.03 M Na_2MoO_4 at pH 9.5 [42].

3.3. Properties of nanocrystalline Ni-Mo alloys

3.3.1. Corrosion properties of nanocrystalline Ni-Mo alloys

Corrosion resistance of nanocrystalline materials is of a great importance in assessing a wide range of potential future applications. To date, a few researches have addressed this issue. Ni-Mo alloys have been studied for their corrosion resistance especially in the media where they are used as cathodes for hydrogen evolution [34]. As indicated previously, Ni-Mo alloys are of excellent corrosion resistance especially in the aqueous solutions containing chloride ions [31]. As for Ni-Mo nanocrystalline alloys, they showed promising protective characteristics evidenced by polarization resistance of about 3.5-17 kΩ. While polarization curves being obtained for Ni-Mo nanocrystalline alloys being immersed in 0.5 M NaCl for various periods as shown in Figure 10 and 11, indicated that at the beginning the alloy with higher Mo content (27-30wt%) having a less negative potential (-0.014V) vs. Ag/AgCl than that for the alloy containing lower Mo content (13-15 wt%) recording a potential of about -0.749V vs. Ag/AgCl. As the immersion period increased, the corrosion potential moved towards more electronegative values, down to about -0.93 V vs. Ag/AgCl, regardless the alloy composition [43]. While in the deaerated hydrochloric solutions, nanocrystalline Ni-Mo alloys being deposited from citrate solution (pH 8.5-9.5) show a large passivation domain without any pitting. The corrosion currents as well as the passivation currents were higher than for the bulk conventional Ni-Mo alloy (Hastelloy B) and decreased when the Mo content in these alloys is increased [43].
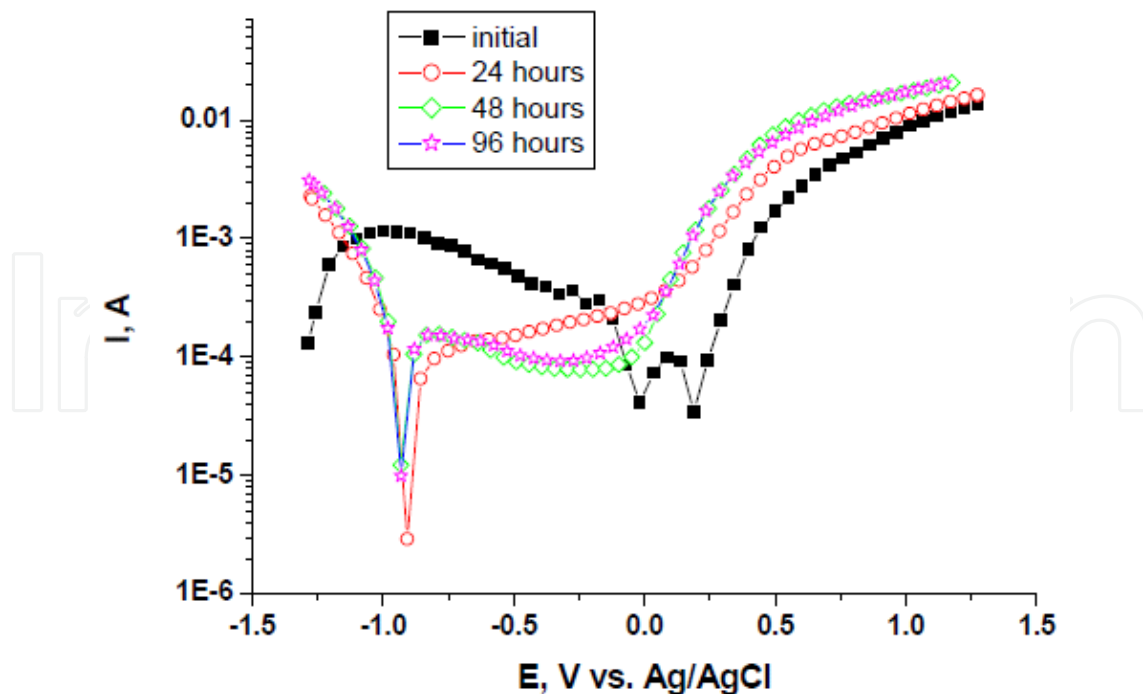

Figure 10. Polarization curves in semilogarithmic coordinates for Ni-Mo alloy (27-30% Mo) deposit in 0.5 M NaCl for various periods of continuous immersion (25 °C, 5 mV/s; geometrical surface of WE-0.63585 cm^2) [43].
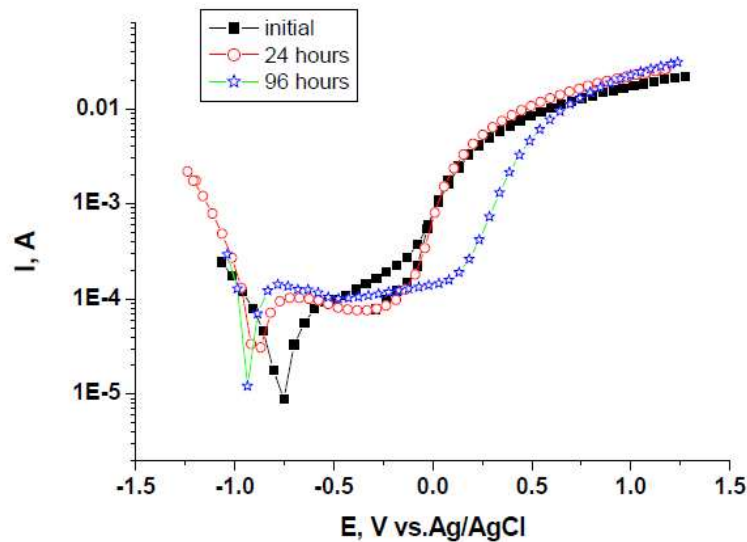
Figure 11. Polarization curves in semilogarithmic coordinates for Ni-Mo alloy (13-15% Mo) deposit in 0.5 M NaCl for various periods of continuous immersion (25 °C, 5 mV/s; geometrical surface of WE-0.63585 cm^2) [43].

3.3.2. Electrocatalytic reactivity for hydrogen evolution

Nanocrystalline Ni-Mo alloys are known for their premium electrocatalytic properties as the presence of molybdenum in these materials apparently increases their catalytic activity. Ni-Mo alloy coatings electrodeosited from pyrophosphate-sodium bicarbonate bath possess high catalytic activity for hydrogen evolution in the NaOH solutions. Their stability in the 1 M NaOH at 25°C under the condition of the reverse polarization are of much better activity toward hydrogen evolution reaction than pure Ni electrode as the overpotential for Ni-Mo electrodeposited alloys was recorded as -1.3V vs. SCE at j = -0.3 Acm^{-2} compared to -1.66 V vs.SCE for Ni electrode [44, 45].

4. Electrodeposition of Ni-Mo nano composites

Broad application of nickel-based composite coatings in electrochemistry is due to the highly catalytic activity in electrocatalytic hydrogen evolution (HER) and electrocatalytic oxygen evolution (OER) as well as good corrosion resistance of nickel in aggressive environments [46]. In order to improve the properties of these materials, and enhance their catalytic activity, various modifications could be applied, such as alloying with other elements, incorporating

composite components. All these modifications aimed at obtaining the electrodes with very developed, rough or porous electrode surface. Many types of particles were used to improve mechanical, physicochemical or electrocatalytic properties of composite coatings, like carbides, silicides, nitrides, and oxides [47, 48]. Recent research in electro deposition suggested a technique involving codeposition of metallic particles to form electrodeposited metal matrix/metal particle composites [49]. Among these composites are those containing metals like Al, Ti, V, Mo which could not be directly deposited from aqueous solutions. Incorporating such powdered components to the metal matrix leads to obtain a new kind of composite material which could be applied as electrode materials [50- 53]. Ni-based binary composite coatings like Ni–Mo, Ni–Zn, Ni–Co, Ni–W, Ni–Fe and Ni–Cr were tried for hydrogen electrodes; out of these electrodes, Ni–Mo was found to be best and most stable electrode with an overpotential of 0.18 V in 6 M KOH solutions [54]. Also according to Kubisztal et al. [55] electrolytic Ni–Mo and Ni–Mo–Si coatings were prepared by codeposition of nickel with silicon and molybdenum powders from a nickel bath in which Mo and Si particles were suspended by stirring. Composite coatings are characterized by very porous surface in comparison with nickel coating after the same thermal treatment. Ni–Mo composite coatings, obtained by electrodeposition of Ni with Mo particles on a steel substrate from the nickel bath containing suspended Mo powder, showed pronounced improvement in the electrochemical performance for HER in an alkaline environment compared to nickel electrode [47, 55]. The molybdenum content and the thickness of the Ni–Mo composite coatings change between 28–46 wt%, and 100–130 nm, respectively depending on the deposition current density. Ni–Mo electrodeposits were characterized by larger surface than the Ni electrodeposits. According to Jovic et al. [56], improved performances are to be expected if a composite compact layer of Ni and some Mo oxides could be prepared by the simultaneous electrodeposition of Ni and MoO_3 from an electrolyte solution in which MoO_3 particles are suspended. It seems a unique way for solving the problem of porosity of electroplated Ni–Mo coatings and low mechanical stability of thermally prepared Ni–Mo catalysts.

Ni–Mo nanocomposite coatings (18–32 nm) were prepared by electrodeposition of nickel from a nickel salt bath containing suspended Mo nanoparticles (Figure 12), by Abdel-Karim et al [57]. All the coatings have been deposited under galvanostatic conditions using current densities in the range 5–80 mA/cm^2. According to structural investigation carried out by X-ray diffraction, the obtained coatings consisted of crystalline Mo phase incorporated into Ni matrix (Figure13). The molybdenum content diminished with increasing the deposition current density and ranged between ~6 and ~17% Mo. Table 4 summarizes the corrosion properties of Ni-Mo composites examined in a remarkable deterioration in the corrosion resistance of Ni–Mo composites was observed with the increase of Mo content due to crystallite size-refining and surface roughness effect. Electrocatalytic effect for hydrogen production was improved mainly as a result of increasing the surface roughness and thus providing more accessible surface area.

According to Low and Walsh [58], many operating parameters influence the quantity of incorporated particles, including current density, bath agitation and electrolyte composition. It has been suggested that the transport of particles is due to electrophoresis,

mechanical entrapment, adsorption, and convection–diffusion. The current density has been found to influence the amount of alumina nanoparticles incorporated into electrode-posited nickel. An increase in current density resulted in a rough surface microstructure and lead to less Al_2O_3 nanoparticles being incorporated in the metal deposit. The trend of decreasing the molybdenum content in Ni–Mo composites as a result of raising the applied current density has been also reported by Kubisztal et al. [55]. This phenomenon could be due to the fact that the amount of Mo powder incorporated in the composite depends on the rate of mass transport. At lower current densities Mo powder has longer time to reach the Ni matrix and form Ni–Mo composite. Whereas, at higher current densities, the Ni layers grow faster and less time is allowed for Mo powder to be transferred to the Ni matrix [54]. Another explanation for the same phenomenon is that by increasing the current density, a strong electric field is produced which in turn creates a partial desorption of nickel ions on the surface of Mo particles [59, 60]. The Ni crystallite size was reduced from ~32 to ~18 nm as the current density was decreased from 80 to 5 mA/cm². These values are less than that for Ni crystallites (62 nm) reported by Panek and Budniok [59]. This fact could be explained by the incorporation of metallic powder particles into the nickel matrix and the influence of the deposition current density. When electrically conductive parti-cles are embedded into the coating, they effectively become a part of the cathode and act as nucleation sites for the Ni matrix. A structure refinement occurs relative to pure Ni coatings due to the periodic nucleation and growth from the surface of the particles.

The generally accepted mechanism of the HER in alkaline solution is based on the following steps:

$$M + H_2O + e \rightarrow MH_{ads} + OH^- \tag{6}$$

$$MH_{ads} + H_2O + e \rightarrow H2 + M + OH^- \tag{7}$$

$$2\,MH \rightarrow\ H_2 + 2\,M \tag{8}$$

where (1) is the proton discharge electrosorption (Volmer reaction), which is followed by electrodesorption step (2) (Heyrovsky reaction) and/or H recombination step (3) (Tafel reaction). According to general models for HER mechanisms, the Volmer–Heyrovsky and Tafel reaction mechanism, reactions (1)–(3), may display three different slopes: 116.3, 38.8 or 29.1 mV dec⁻¹ at 20 °C. When Heyrovsky reaction is the rate determining step, r.d.s., the slope is 38.8 mV dec⁻¹ and when the Tafel reaction is the r.d.s. slope is 29.1 mV dec⁻¹. When the slope of 116.3 mV dec⁻¹ is observed, it is impossible to distinguish which step is the rate determining one. However, as the surface coverage by adsorbed hydrogen should increase with the increase in negative overpotential, the rate limiting step should be that of Heyrovsky [54, 60].
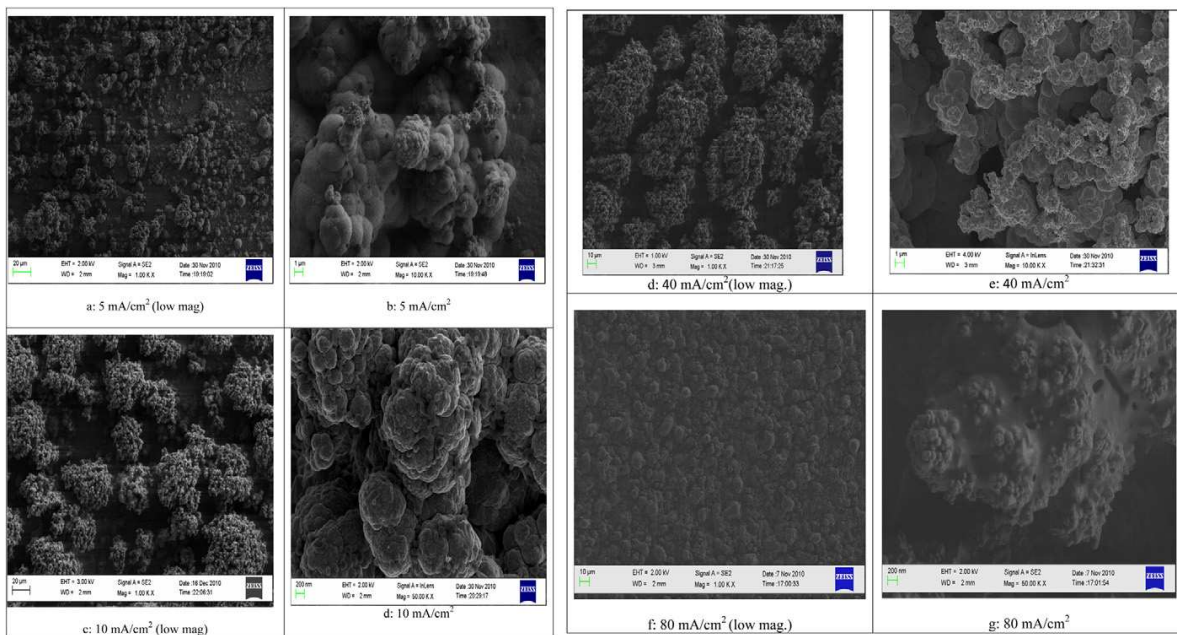
Figure 12. SEM micrographs for electrodeposited layers of Ni–Mo composites [57].
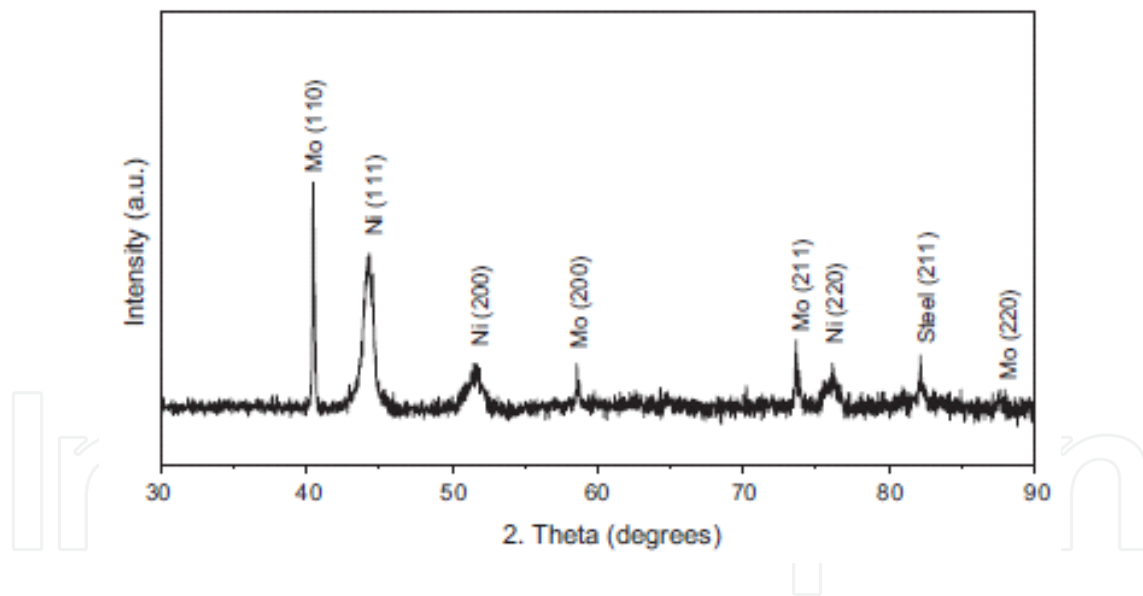
Figure 13. XRD of electrodeposited Ni-Mo nanocomposites [57].

4.1. Corrosion properties of electrodeposited Ni–Mo composites

From Table 4, electrodeposited Ni–Mo composites prepared by R. Abdel-karim et al et al [57] showed higher corrosion rates (0.035–1.795 mm/y) compared to the corrosion rates of Ni–Mo electrodeposited alloys (4.7–8.3 ×10^{-3} mm/y) [9]. This result would be attributed to the non-homogeneity and the rough surface of the Ni–Mo composites compared to the surface of Ni–Mo alloys. The highest electrocatalytic activity is detected for Ni–Mo composite containing

~6% Mo as well as the high surface roughness value (5.35 μm). The obtained results are in agreement with the results obtained by Panek and Budniok [59] and would indicate that both factors (Mo content and surface roughness) influence the electrocatlaytic behavior of Ni–Mo composites. The decrease of one of these two factors would lead to reduction in the electrocatalytic activity as for hydrogen evolution reaction. According to Kubisztal et al. [55], the main contribution toward the electrocatalytic activity of Ni–Mo composites is attributed to the increase in the actual surface area due to higher surface roughness. Mo particles, while embedded in the Ni matrix, produce a moderate increase in the catalytic effect in the point of contact.

Compared to previous work [40] and from table 5 [57], the Ni–Mo composite offers a higher electrochemical activity toward hydrogen evolution reaction (HER) than that of Ni–Mo alloys, with the sample containing 17% Mo had the lowest overpotential (−0.725 mV) at j = −1.5 mA/cm^2. These observations are in agreement with Popczyk [60].

Plating current density, mA/cm^2	Mo content, %wt	Ecorr, mV	Icorr, μm/cm^2	Corrosion rate, mm/y
5	14.6	-435	42.7	0.5
10	17.22	-512	153.5	1.795
20	16.7	-752	105.6	1.236
80	6.4	-356	2.94	0.035

Table 4. Corrosion properties of electrodeposited Ni-Mo nanocrystalline composites

Plating current density, mA/cm^2	Mo content, %wt	Roughness, Rq, μm	Ni crystallite size, nm	Cathodic mV/decade	Evs SCE(V) at j= -1.5 mA/cm^2
5	14.6	0.965	18.3	-115.2	-1
10	17.2	25.6	25.6	-142.7	-0.725
20	16.7	28.5	28.5	-118	-0.92
80	6.35	32.1	32.1	-34.9	n.a

Table 5. Electrocatalyric properties of electrodeposited Ni-Mo nanocrystalline composites

5. Nano-porous alumina formation

Nanoporous alumina films "AAO" produced during electrochemical anodization of aluminum has been studied for many years, and has continued to attract interest from various researchers because of its unique chemical and physical properties. These unique properties have made it possible for a wider application such as electronic devices, magnetic storage disks, sensors in hydrogen detection, adsorption of volatile organic compounds; biodevices; and in drug delivery, etc [61- 63].

The advantages of using the AAO membrane as a template are firstly, that it allows the diameter of the nanowires, nanorods and nanotube to be tailored to the respective pore size in the membrane (Figure 14) [63]. Secondly, it ensures that the growth of the nanocrystal (nanowire, nanorod, nanotube) is aligned within the high aspect ratio nano-channel which is also perpendicular to the substrate surface at the base of the membrane. A wide variety of materials that include metals, oxides, conductive polymers and semiconductors can then be deposited into the pores of the membrane. Then a suitable formation mechanism can be used to generate nanowires, nanorods (short nanowires) and nanotubes. The dimensions of which can be controlled by adjusting the template pore geometry and the formation parameters [64].
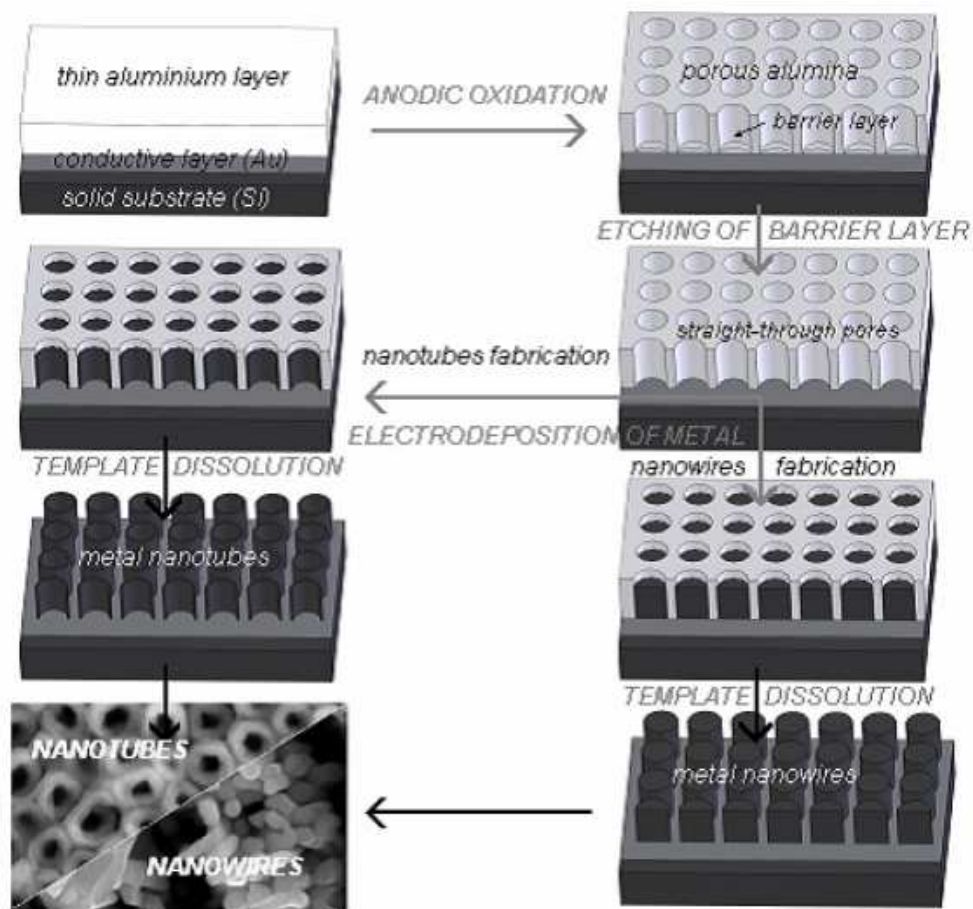

Figure 14. Template Assisted Growth of Nanowires and Nanorods [63]

Electrodeposition of nanoscale materials in the pores of a self- ordered nanochannel matrix is of relatively low cost. Furthermore, electrodeposition is a fast process for the fabrication of large arrays of nanostructures with a very large aspect ratio, which is not possible with standard lithographic techniques [65]. Electrochemical synthesis in a template is taken as one of the most efficient methods in controlling the growth of nanowires and has been used to produce a variety of metal nanowires [66].

AAO template is an ideal mold because it possesses many desirable characteristics, including tunable pore dimensions, good mechanical property, and good thermal stability. Moreover, especially for metal nanowires, the AAO template has been proved to be a cheap and high yield technique to produce large arrays of metals nanowires by the electrodeposition. This oxide has ordered hexagonal cells, of which every cell contains a cylindrical pore at its center. The pore diameter, cell size and barrier layer thickness can be controlled by anodizing voltage and the depth of pore by anodizing time [61]. Masuda et al. [64] has shown that AAO membranes with large pore sizes can be used in optical devices, particularly in the infra-red region of the spectrum.

The controlled placement of nano-dots on a substrate can be achieved with great accuracy using electron beam lithography. The major disadvantages of using this technique are the high capital cost of the equipment and the long exposure times which result in a low production output. An alternative process for the large scale fabrication of nano-dots on a semiconductor substrate uses an AAO membrane as an evaporation mask. The membrane provides an array of uniformly sized pores and site controlled pore locations where the nano-dots can be deposited. Before being used as a mask, the barrier layer is removed from the AAO membrane using a suitable etching technique, leaving a through pore structure or nano-channel. The major advantage of manufacturing nano-dot arrays using an AAO membrane is that the membrane can be used as a template. The template provides the precise location of individual pores in a high-density pore array without the need for expensive lithographic processes. The potential technological application of nano-dots is in the fabrication of ultra-small electronic devices, ultrahigh-density recording media, and nano-catalysis applications [64].

5.1. Nano-porous alumina formation mechanism

The formation process of the nano-porous oxide layer is a complex process that produces a self- organized hexagonal pore array, these hexagonal honeycomb structures have been reported by several researchers [67-73]. The porous structure consists of a thin non porous oxide layer of constant thickness that is adjacent to the metal substrate that continually regenerates at the base of the pore while the pore wall is being created, this wall increases in height with time. The particular electrolyte, its concentration, the anodic voltage and bath temperature are the main parameters in determining the pore size and the distance between pores [74].

Typical electrolytes used to produce this type of oxide layer have a pH that is less than 5, and slowly dissolve the forming oxide layer. Examples of the acids used are sulfuric, phosphoric and oxalic. However; mixtures of organic and inorganic acids have also been used. The properties of the electrolyte are important in the formation of porosity and permeability. Electrolytes that are composed of less concentrated acids tend to produces oxide coatings that are harder, thicker, less porous and more wear resistant than those composed of higher concentrated acids. But the most important factor that must be considered when forming the porous oxide is the electrolyte's ability to sustain a significant flow of Al^{3+} ions from the metal substrate into the electrolyte. There are two mechanisms that are responsible for the loss of Al^{3+} ions from the metal substrate. The first is by the direct expulsion of ions by the applied

electrical field and the second is the dissolution of the forming oxide layer. In addition, if there are regions of high current flows when the electric field is applied, an increased dissolution rate can result (field assisted dissolution) [75].

The origin of pore nuclei and the exact mechanism of pore nucleation are still largely unknown. Several formation models have been proposed [76, 77]; one model explains that pore nucleation results from an electric field assisted local chemical dissolution [78] at the electrolyte/oxide interface and oxide generation at the metal/oxide interface. For electrolytes with a pH less than 5, there is a significant flow of Al^{3+} ions into the electrolyte and as a consequence there are regions where the formation of new oxide at the oxide/electrolyte interface is unstable. This regional instability produces variations in the applied electrical field; this in turn results in an increased dissolution rate [78, 79]. This mechanism produces an underlying metal/oxide and oxide/electrolyte interfaces that consist of a large numbers of hemispherical depressions per cm^2 that corresponds to the pores density. In these depressions the electrical field tends to be more concentrated due to the focusing effect of the hemispherical shape, hence the increased dissolution rate. [80]. In contrast, the electrical field is fairly constant over the surface of the barrier layer formed in an electrolyte with a pH greater than 5, where the oxide thickness is uniform and stable. These hemispherical depressions form the foundations of the resulting pore structures. The location of these depressions is also influenced by the initial surface topography, surface imperfections such as impurities, pits, scratches, grain boundaries and surface treatments prior to anodization [81]. Patermarakis et al. [82] proposed a pore nucleation model that results from the spontaneous recrystallization of the unstable rare lattice of oxide formed at the surface of the Al adjacent to metal/oxide interface to a more stable denser nano-crystalline oxide located in the oxide layer. The resulting recrystallization ruptures in the surface and produces regions of rarefied oxide between nanocrystallites (anhydrous/amor-phous). It is in these regions that pore nuclei form. Earlier studies by Habazaki et al. [77] indicated the potential for the enrichment of alloying elements, dopants and/or impurities in the Al substrate adjacent to the metal/oxide interface. The enrichment layers were found to be about 1 to 5 nm thick immediately beneath the metal/oxide interface and were a consequence of the oxide growth. These enrichment layers may also be involved in the initiation of changes within the oxide layer that promote pore nucleation. In a recent investigation by Zaraska et al. [78], the presence of alloying elements in an Al alloy (AA1050) not only slowed the rate of oxide growth but also influenced structural features such as porosity, barrier layer thickness, pore diameter and pore density of the forming oxide layer.

In the early stages of the anodization process Al^{3+} ions migrate from the metal across the metal/oxide interface into the forming oxide layer [83]. Meanwhile O^{2-} ions formed from water at the oxide/electrolyte interface travel into the oxide layer. During this stage approximately 70% of the Al^{3+} ions and the O^{2-} ions contribute to the formation of the barrier oxide layer [79], the remaining Al^{3+} ions are dissolved into the electrolyte. This condition has been shown to be the prerequisite for porous oxide growth, in which the Al-O bonds in the oxide lattice break to release Al^{3+} ions [80]. During the oxide formation the barrier layer constantly regenerates with further oxide growth and transforms into a semi-spherical oxide layer of constant thickness that forms the pore bottom, as shown in Figure 15 [75].
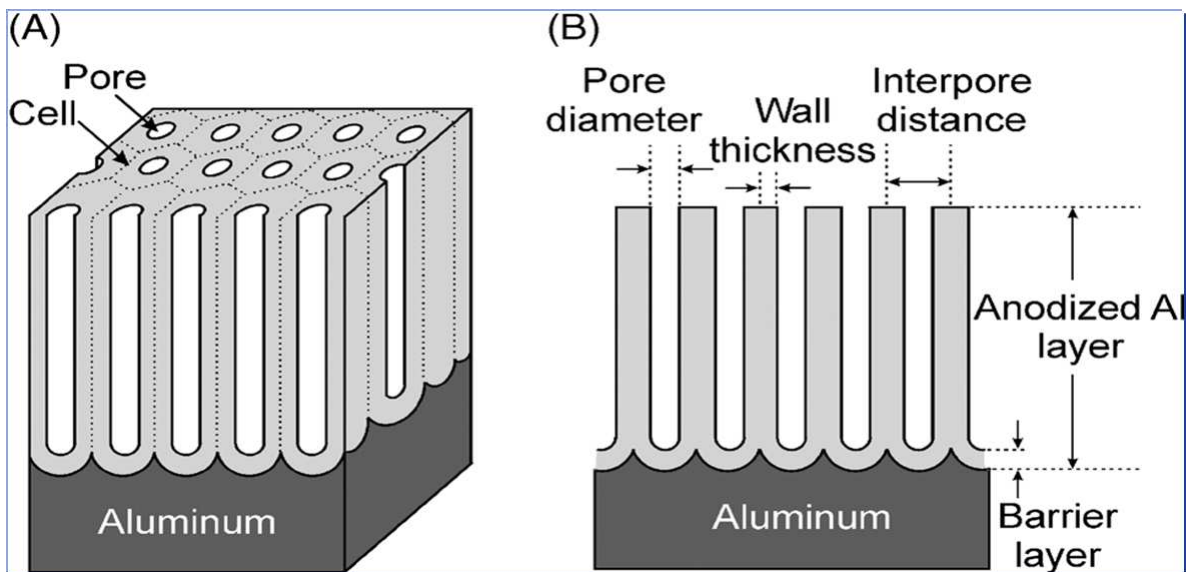
Figure 15. Schematic structure of anodic porous alumina (A) and a cross-sectional view of the anodized layer (B) [75].

During the formation of the porous oxide layer the anodic Al dissolution reaction is presented by:

$$2Al \rightarrow 2Al^{3+} + 6e^- \tag{9}$$

$$6H^+ + 6e^- \rightarrow 3H_2 \tag{10}$$

$$2Al + 3O^{2-} \rightarrow Al_2O_3 + 6e^- \tag{11}$$

$$2Al^{3+} + 3H_2O \rightarrow Al_2O_3 + 6H^+ \tag{12}$$

Sum of the separate reactions at electrode: (Overall anodization of Al equation)

$$2Al + 3H_2O \rightarrow Al_2O_3 + 3H_2 \tag{13}$$

The steady state growth results from the balance between the field-enhanced oxide dissolution at the oxide/electrolyte interface at the base of the hemispherical shaped pores where the electric field is high enough to propel the Al^{3+} ions through the barrier layer and the oxide growth at the metal/oxide interface resulting from the migration of O^{2-} and OH^- ions into the pore base oxide layer, as in Figure 16. This also explains the dependence of the size of the pore diameter to the electric field produced by the anodizing voltage. It should also be noted that the electric field strength in the pore walls is too small to make any significant contribution to the flow of ions.

The oxidation takes place over the entire pore base and the resulting oxide material grows perpendicular to the surface, neighboring pore growth prevents growth in any other direction. The vertical growth of the pore wall creates a columnar structure with a high aspect ratio that contains a central circular channel. This channel extends from the base of the pore to the surface of the oxide layer [81]. This upward growth of the pore wall was recently investigated by Garcia-Vergara et al. [86] in which a tungsten tracer was placed into an initial oxide layer formed by an initial anodization step. During the next stage of anodization, the position of the tracer was monitored and found to travel from the metal/oxide interface of the barrier layer located at the base of the pore towards the growing wall structure. This flowing motion of the tracer was credited to the mechanical stresses being generated by the continued formation of new oxide within the pore base and the repulsive forces set up between neighboring pores during the growth of the wall structure. These forces resulted from the volume expansion (by a factor of 2) during the oxidation of Al to alumina. This volumetric expansion factor results from the difference in the density of Al in alumina (3.2 g cm^{-2}) and that of metallic Al (2.7 g cm^{-2}). This volumetric oxide expansion at the metal/oxide interface also contributes to the hemispherical shape of the pore base. However, under normal experimental conditions, the volumetric expansion factor is less than 2. This is due to the hydration reaction that occurs at the oxide/electrolyte interface which results in the dissolution and thinning of the oxide layer.
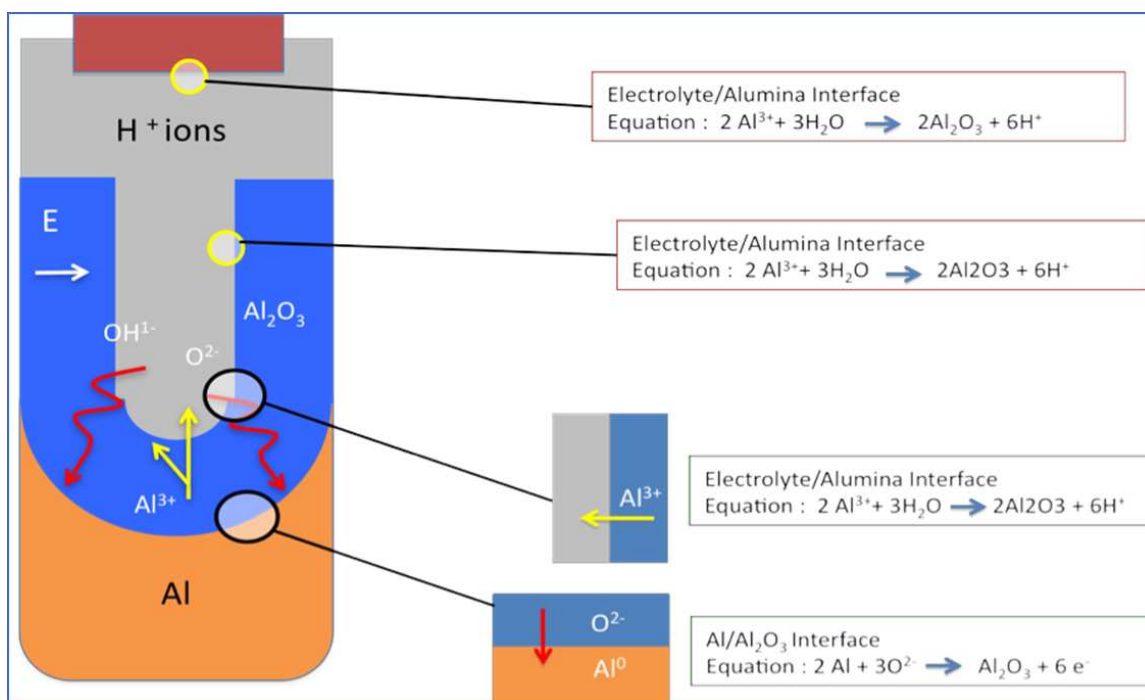

Figure 16. Schematic of ion movement during pore formation [81].

The volumetric growth of the oxide layer is also dependent upon the type of electrolyte (this effect is more evident when using phosphoric or sulfuric acids), the electrolyte concentration and the electric field created by the anodizing voltage. Furthermore, a research investigation by Li et al. [85] has shown that a volume expansion factor of 1.4 could be achieved under

optimal anodizing parameters, independent of the electrolyte used. The porous oxide layer thickness and hence pore height can grow to many times the height of the barrier layer. It is usually during this oxide growth that electrolyte anions can integrate into the forming porous structure near the oxide/electrolyte interface, while pure alumina is predominantly found in layers close to the metal/oxide interface. It is also possible for voids to form in the pore walls during the growth of the oxide layer. Possible causes of these voids range from oxygen evolution during oxide formation to localized defects in the barrier layer. These defects produce a condensation effect that involves cations and/or metal vacancies at the metal/oxide interface, which subsequently become detached, and form the void.

Diggle et al. [86].discussed the contradictory research results of the period. For example, the non- porous barrier layer was regarded as amorphous and anhydrous, while the porous layer had been found to be both amorphous and crystalline. In the case of the barrier layer, under normal anodization conditions the layer will be amorphous. However, studies by Uchi et al. [87] have shown that with the right growth conditions it was possible to have amorphous or crystalline Al oxide being produced during anodization. To form a crystalline oxide structure; an Al substrate was first immersed in boiling water to form a hydrous oxide layer [oxy-hydroxide with excess water ($AlOOH.H_2O$)]. The substrate was then anodized in a neutral borate solution at high temperatures, during which Al^{3+} ions move from the metal substrate to the hydrous oxide interface, where they combine and transform the hydrous oxide to crystalline Al_2O_3. Some of the contradictory evidence of the earlier works discussed by Diggle et al. [86] of the porous layer could be explained by the work of De Azevedo et al. [88]. In this study the structural characteristics of doped and un-doped porous Al oxide, anodized in oxalic acid was investigated using X-ray diffraction (XRD). The XRD patterns for the un-doped samples revealed several peaks associated with Al and Al_2O_3 crystalline phases on top of a broad peak that was approximately centered on the 2θ angle of 25°. This broad peak indicated that the synthesized layer was a highly disordered and/or amorphous Al oxide compound.

6. Conclusions

- One of the most important aspects of self-assembly lies in the capability of producing uniform structures over a large area using conventional electrodepsotion and anodizing processes.

- Nanostructured Ni-Fe alloys, produced by electro-deposition technique provide material with significant improved strength and good magnetic properties, without compromising the coefficient of thermal expansion.

- Due to better anticorrosive in several aggressive environments, mechanical and thermal stability characteristics of Ni-Mo alloys, the electro deposition of these alloys plays an important role. Broad application of nickel-based composite coatings in electrochemistry is due to the highly catalytic activity in electrocatalytic hydrogen evolution (HER) and electrocatalytic oxygen evolution (OER) as well as good corrosion resistance of nickel in aggressive environments.

- AAO template has been proved to be a cheap and high yield technique to produce large arrays of metals nanowires with tunable pore dimensions, good mechanical property, and good thermal stability by the electrodeposition.

Author details

R. Abdel-Karim[1] and A. F. Waheed[2]

1 Department of Metallurgy, Faculty of Engineering, Cairo University, Giza, Egypt

2 Department of Metallurgy, Nuclear Research Center, Cairo, Anshas, Egypt

References

[1] Luther, W. Industrial Application of Nanomaterials- Chances and Risks, Future Technologies Division of VDI Technologiezentrum GmbH, (2004).

[2] Aliofkhazraei, M. Nanocoatings, chapter 1, Springer, (2011).

[3] Gleiter, H. Nanostructured Materials: Basic Concepts and Microstructure. Acta Materialia (2000). , 48(1), 1-29.

[4] Peuloro, S, & Lincot, D. Cathodic Electrodeposition from Aqueous Solution of Dense or Open-structured Zinc Oxide Films. Advanced. Materials (1996). , 8, 166-170.

[5] Koch, C. C. Nanostructured Materials: Processing, Properties and Applications, William Andrew Publishing; 2 nd edition, (2007).

[6] Bockris, J. O'M. Fundamental Aspects of Electrocrystallization, Plumn Press, New York, 3 rd edition, first published; (1967).

[7] Uve, E. Materials Processing Handbook, chapter 22, CRC; (2007).

[8] Seo, M. H, Kim, D. J, & Kim, J. S. The Effects of pH and Temperature on Ni-Fe-P Alloy Electrodeposition from a Sulfamate Bath and the Material Properties of the Deposits. Thin Solid Films (2005)., 489 (1-2), 122-129.

[9] Sam, S, Fortas, G, Guittoum, A, Gabouze, N, & Djebbar, S. Electrodeposition of NiFe Films on Si (1 0 0) Substrate, Surface Science (2007). , 601(18), 4270-4273.

[10] Abdel-karim, R, Reda, Y, Muhammed, M, Raghy, S, Shoeib, M, & Ahmed, H. Electrodeposition and Characterization of Nanocrystalline Ni-Fe Alloys. Journal of Nanomaterials 2011; (2011). Article ID 519274, 8 pages.

[11] Brenner, A. Electrodeposition of Alloys, chapter 1, Academic Press, New York, NY, USA; (1963).

[12] Afshar, A, Dolati, A. G, & Ghorbani, M. Electrochemical Characterization of the Ni-Fe Alloy Electrodeposition from Chloride-Citrate-Glycolic Acid Solutions", Materials Chemistry and Physics (2002). , 72(2), 352-258.

[13] Krause, T, Arulnayagam, L, & Pritzker, M. Model for Nickel-Iron Alloy Electrodeposition on a Rotating Disk Electrode. Journal of the Electrochemical Society(1997). , 144(6), 953-960.

[14] Mc Crea, J. L, Palumbo, G, Hibbard, G. D, & Erb, U. Properties and Applications for Electrodeposited Nanocrystalline Fe-Ni Alloys. Review of Advanced Material Science (2003). , 5, 252-258.

[15] Krstic, V, Erb, U, & Palumbo, G. Effect of Porosity on Young's Modulus of Nanocrystalline Materials. Scripta Metallurgia and Materiala (1993). , 29, 1501-1504.

[16] Zugic, R, Szpunar, B, Krstic, V. D, & Erb, U. Effect of Porosity on the Elastic Response of Brittle Materials: An Embedded-atom Method Approach. Philosophical Magazine A- Physics of Condensed Matter Structure Defects and Mechanical Properties (1997). , 75(4), 1041-1055.

[17] Brooks, I. Synthesis and Mechanical Properties of Bulk Quantities of Electrodeposited Nanocrystalline Materials, University of Toronto. Ph. D thesis, Canada, (2012).

[18] Sherik, M, Ajwad, H, Rasheed, A. H, Jabran, A, & Ortiguerra, R. G. Adhesion and Corrosion Performance of Nanostructured Nickel and Cobalt-based Coatings. CORROSION 2008, March New Orleans LA.; (2008). Document ID 08025, 16-20.

[19] Shangyu, W. Electrochemical Properties of Nanocrystalline Nickel and Nickel-Molybdenum Alloys. Ph.D dissertation, Queen's University, Kingston, Ontario, Canada; (1997).

[20] Alves, H, Ferreira, M. G. S, & Koster, U. Corrosion Behavior of Nanocrystalline (Ni70Mo30)90B10 Alloys in 0.8 M KOH Solution. Corrosion Science (2003). , 45, 1833-1845.

[21] Egberts, P, & Hibbard, G. D. Mesoscale. Compositionally Modulated Nanocrystalline Ni-Fe Electrodeposits for Nanopatterning Applications. Journal of Nanomaterials 2008; (2008). Article ID 858235.

[22] Ramanujan, R. V. Nanostructured Electronic and Magnetic Materials. S̄adhan̄a (2003)., 1&2, 81-90.

[23] Suryanarayana, C, & Koch, C. C. Nanocrystalline Materials- Current Research and Future Directions. Hyperfine Interactions (2000). , 130, 5-44.

[24] Reda, Y. Preparation and Characterization of Electrodeposited Nano-crystalline Fe-Ni Alloys. Ph. D dissertation, Cairo University, Egypt; (2010).

[25] Halim, J. Electrodeposition and Characterization of Nanocrystaline Ni-Fe Alloys. B.Sc graduation project, Cairo University; Egypt (2009).

[26] Garibay, V, Diaz, L, Paniagua, A, & Palacios, E. Nanostructured Materials Development with Applications to the Petroleum Industry. Acta Microscopia (2000). , 18, 52-58.

[27] Huang, T, Huang, W, Huang, J, & Ji, P. Methane Reforming Reaction with Carbon Dioxide Over SBA-15 Supported Ni-Mo Bimetallic Catalysts, Fuel Process. Technology (2011). , 92(10), 1813-2126.

[28] Schulz, R, Huot, J, & Trudeau, M. Nanocrystalline Ni-Mo Alloys and Their Application in Electrocatalysis. Journal of Material Research (1994). , 9(11), 2998-3008.

[29] Jin-zhao, H, Zheag, X, & Hai-ling, L. Effects of Sputtering Conditions on Electrochemical Behavior and Physical Properties of Ni-Mo Alloy Electrode", Transactions of Nonferrous Metals Society of China (2006). , 16(5), 1092-1096.

[30] Kedzierzawski, P, Oleszak, D, & Janik-czachor, M. Hydrogen Evolution on Hot and Cold Consolidated Ni-Mo Alloys Produced by Mechanical Alloying. Materials Science and Engineering A (2001)., 300(1-2), 105-112.

[31] Donten, M, Cesiulis, H, & Stojek, Z. Electrodeposition of Amorphous/nanocrystalline and Polycrystalline Ni-Mo Alloys from Ayrophosphate Baths. Electrochemica Acta (2005). , 50(6), 1405-1412.

[32] Clark, D, Wood, D, & Erb, U. Industrial Applications of Electrodeposited Nanocrystals", Nanostructured Materials (1997)., 9(1-8), 755-758.

[33] Robertson, A, Erb, U, & Palumbo, G. Practical applications for Electrodeposited Nanocrystalline Materials. Nanostructured Materials (1999)., 12(5-8), 1035-1040.

[34] Raj, I. A, & Vekatesan, V. K. Characterization of nickel-molybdenum and nickel-molybdenum-iron alloy coatings as cathodes for alkaline water electrolysers. International Journal of. Hydrogen Energy (1988). , 13(4), 215-223.

[35] Palumbo, G, Gonzalez, F, & Brennenstuhl, A. M. In-situ Nuclear Steam Generator Repair Using Electrodeposited Nanocrystalline Nickel. Nanostructured Materials (1997)., 9(1-8), 737-746.

[36] Robertson, A, Erb, U, & Palumbo, G. Practical Applications for Electrodeposited Nanocrystalline Materials. Nano structured Materials (1999). , 12, 1035-1040.

[37] Sundaramurthy, V, Dalai, A. K, & Adjaye, J. Comparison of P-containing γ-Al2O3 Supported Ni-Mo Bimetallic Carbide, Nitride and Sulfide Catalysts for HDN and HDS of Gas Oils Derived from Athabasca Bitumen. Applied Catalysis A (2006)., 311(1-2), 155-163.

[38] Borowiecki, T, Gac, W, & Denis, A. Effects of Small MoO3 Additions on the Properties of Nickel Catalysts for the Steam Reforming of Hydrocarbons: III. Reduction of Ni-Mo/Al2O3 Catalysts. Applied Catalysis A (2004)., 270(1-2), 27-36.

[39] Chassaing, E, Roumegas, M. P, & Trichet, M. F. Electrodeposition of Ni-Mo Alloys with Pulse Reverse Potentials. Journal of Applied Electrochemistry (1995). , 25(7), 667-670.

[40] Halim, J, Abdel-karim, R, Raghy, S, Nabil, M, & Waheed, A. Electrodeposition and Characterization of Nanocrystalline Ni-Mo Catalysts for Hydrogen Production. Journal of Nanomaterials 2012; (2012). Article ID 845673, 10 pages.

[41] Podlaha, E. J, & Landolt, D. I. An Experimental Investigation of Ni-Mo Alloys. Journal of Electrochemical Society (1996). , 143(3), 885-892.

[42] Podlaha, E. J, & Landolt, D. II.A Mathematical Model Describing the Electrodeposition of Ni-Mo Alloys. Journal of Electrochemical Society (1996). , 143(3), 893-899.

[43] Chassaing, E, & Portail, N. Characterization of Electrodeposited Nanocrystalline Ni-Mo Alloys. Journal of Applied Electrochemistry (2005). , 34(1), 1085-1091.

[44] Prioteasa, P, & Anicai, L. Synthesis and Corrosion Characterization of Electrodeposited Ni-Mo alloys Obtained from Aqueous Solutions, U.P.B. Science Bulletin B (2010). , 72(4), 11-24.

[45] Krstajic, N. V, & Jovic, V. D. Electrodeposition of Ni-Mo Alloy Coatings and their Characterization as Cathodes for Hydrogen Evolution in Sodium Hydroxide Solution", International Journal of Hydrogen Energy (2008). , 33(6), 3676-3687.

[46] Niedbala, J. Surface Morphology and Corrosion Resistance of Electrodeposited Composite Coatings Containing Polyethylene or Polythiophene in Ni-Mo Base, Bulletin of Material Science (2011). , 34, 993-996.

[47] Panek, J, & Budniok, A. Study of Hydrogen Evolution Reaction on Nickel-Based Composite Coatings containing Molybdenum Powder", International Journal of Hydrogen Energy (2007). , 32, 1211-1218.

[48] Aruna, S. T. William Grips, V. K., Rajam K. S. Ni-based Electrodeposited Composite Coating Exhibiting Improved Microhardness, Corrosion and Wear Resistance Properties", Journal of Alloys and Compounds (2009). , 468(2009), 546-552.

[49] Lekka, M, Kouloumbi, N, Gajo, M, & Bonora, P. L. Corrosion and Wear Resistant Electrodeposited Composite Coatings. Electrochimica Acta (2005). , 50, 4551-4556.

[50] Naploszek-bilnik, I, Budniok, A, & Lagiewka, E. Electrolytic Production and Heat-treatment of Ni-based Composite Layers Containing Intermetallic phases. Journal of Alloys and Compounds (2004). , 382, 54-60.

[51] Ping, Z, Cheng, G, & He, Y. Ni-P- SiC Composite Coatings Electroplated on Carbon Steel Assisted by Mechanical Attrition. Acta Metallurgica. Sinica. (Engl. Lett.) (2010). , 23(1), 1-10.

[52] Raj, I. A, & Vasu, K. I. Transition Metal-based Cathodes for Hydrogen Evolution in Alkaline Solution: Electrolysis on Nickel-based Electrolytic Codeposites. Journal of Applied Electrochemistry (1992). , 22(5), 471-477.

[53] Jakšić JM., Vojnović M.V., Krstajić N.V. Kinetic Analysis of Hydrogen Evolution at Ni-Mo Alloy Electrodes. Electrochimica Acta (2000). , 45, 4151-4158.

[54] Raj, I. A. Nickel Based Composite Electrolytic Surface Coatings as Electrocatalysts for the Cathodes in the Energy Efficient Industrial Production of Hydrogen from Alkaline Water Electrolytic Cells. International Journal of Hydrogen Energy (1992). , 17(6), 413-421.

[55] Kubisztal, J, & Budniok, A. Study of the Oxygen Evolution Reaction on Nickel-based Composite Coatings in Alkaline Media. International Journal of. Hydrogen Energy (2008). , 33, 4488-4494.

[56] Jovic, B.M, Lacnjeva, U, Jovic, V, Serb, J, & Ni-MoO2 Composite Cathodes for Hydrogen Evolution in Alkaline Solution. Effect of Aging of the Electrolyte for Their Electrodeposition. Journal of Serbian Chemical Society (2012). , 77 (0): 1-21.

[57] Abdel-karim, R, Halim, J, Raghy, S, Nabil, M, & Waheed, A. Surface Morphology and Electrochemical Characterization of Electrodeposited Ni-Mo Nanocomposites as Cathodes for Hydrogen Evolution. Journal of Alloys and Compounds (2012). , 530, 85-90.

[58] Low, C. T, & Walsh, F. C. Electrodeposition of Composite Coatings Containing Nanoparticles in a Metal Deposit. Surface Coating Technology (2006). , 2006, 371-383.

[59] Panek, J, & Budniok, A. Electrochemical Production and Characterization of Ni-Based Composite Coatings Containing Mo Particles. Advanced Review of Material Science (2007). , 201(14), 6478-6483.

[60] Popczyk, M. The Hydrogen Evolution Reaction on Electroctrolytic Nickel-Based Coatings Containing Metallic Molybdenum. Materials Science Forum (2010). , 636-637. 1036-1041.

[61] Eddy, G, Poinern, J, Ali, N, & Fawcett, D. Progress in Nano-Engineered Anodic Aluminum Oxide Membrane Development. Materials (2011). , 4, 487-526.

[62] Hamrakulov, B. Kim In-Soo, Lee M. G., Park B. H. Electrodeposited Ni, Fe, Co and Cu Single and Multilayer Nanowire Arrays on Anodic Aluminum Oxide Template, Transaction of Nonferrous Metals Society of China (2009). , 19, 583-587.

[63] Vorozhtsova, M, Hrdy, R, & Hubalek, J. Vertically Aligned Nanostructures for Electrochemical Sensors. Rožnov pod Radhoštěm. NANOCON, 20 - 22. 10. (2009).

[64] Masuda, H, Yada, K, & Osaka, A. Self-ordering of Cell Configuration of Anodic Porous Alumina with Large-Size Pores in Phosphoric Acid Solution. Jpn. Journal of Applied Physics (1998). , 37, LL1340- 1342.

[65] Kim, J. R, Oh, H, So, H. M, Kim, J. J, Kim, J, Lee, C. J, & Lyu, S. C. Schottky Diodes Based on a Single GaN Nanowire. Nanotechnology (2002). , 2002(13), 701-704.

[66] Mikhaylova, M, Toprak, M, Kim, D. K, Zhang, Y, & Muhammed, M. Nanowire Formation by Electrodeposition in Modified Nanoporous Polycrystalline Anodic Alumina Templates. Mat. Research. Society. Symp. Proceeding (2002). , 704, 155-160.

[67] Cheng-min ShenXiao-gang Zhang, Hu-lin Li," DC Electrochemical Deposition of CdSe Nanorods Array Using Porous Anodic Aluminum Oxide Template", Materials Science and Engineering A (2001). , 303, 19-23.

[68] Li, A. P, Muller, F, Birner, A, Nielsch, K, & Gosele, U. Polycrytalline Nanopore arrays with Hexagonal Ordering on Aluminium. Journal of Vac. Science Technology. A (1999). , 17, 1428-1431.

[69] Li, A. P, Muller, F, Birner, A, Nielsch, K, & Gosele, U. Hexagonal Pore Arrays with a 50-420 Interpore Distance Formed by Self-organisation in Anodic Alumina. Journal of Applied Physics (1998). , 84, 6023-6026.

[70] Zhang, L, Cho, H. S, Li, F, Metzger, R. M, & Doyle, W. D. Cellular Growth of Highly Ordered Porous Anodic Films on Aluminium. Journal of Material Science Letter (1998). , 17, 291-294.

[71] Hou, K, Tu, J. P, & Zhang, X. B. Preparation of Porous Alumina Film on Aluminium Substrate by Anodization in Oxalic Acid. China Chemical Letters (2002). , 13, 689-692.

[72] Kim, Y. S, Pyun, S. I, Moon, S. M, & Kim, J. D. The Effects of Applied Potential and pH on the Electrochemical Dissolution of the Barrier Layer in Porous Anodic Oxide Film on Pure Aluminium. Corrosion Science (1996). , 38, 329-336.

[73] Sullivan, O, Wood, J. P, & Nucleation, G. C. and Growth of Porous Anodic Films on Aluminium. P Roy. Lond. A Mat. A (1970). , 317, 511-543.

[74] Thompson, G. E, Furneaux, R. C, Wood, G. C, Richardson, J. A, & Goode, J. S. Nucleation and Growth of Porous Anodic Films on Aluminium. Nature (1978). , 272, 433-435.

[75] Eftekhari, A. Nanostructured Materials in Electrochemistry. WILEY-VCH Verlag GmbH & Co. KGaA, Weinheim, chapter1, (2008).

[76] Hoar, T. P, & Yahaloom, J. The Initiation of Pores in Anodic Oxide Films Formed on Aluminium in Acid Solutions. Journal of Electrochemical Society (1963). , 110, 614-621.

[77] Habazaki, H, Shimizu, K, Skeldon, P, Thompson, G. E, Wood, G. C, & Zhou, X. Nanoscale Enrichments of Substrate Elements in the Growth of Thin Oxide Films. Corrosion Science (1997). , 39, 731-737.

[78] Zaraska, L, Sulka, G. D, Szeremeta, J, & Jaskula, M. Porous Anodic Alumina Formed by Anodisation of Aluminium Alloy (AA1050) and High Purity Aluminium. Electrochimica Acta (2010). , 55, 4377-4386.

[79] Palbroda, E. Aluminium Porous Growth-II on the Rate Determining Step. Electrochimica Acta (1995). , 40, 1051-1055.

[80] Shawaqfeh, A. T, & Baltus, R. E. Fabrication and Characterization of Single Layer and Muti-layer Anodic Alumina Membrane. Journal of Membrane Science (1999). , 157, 147-158.

[81] Essa, A. K. Porous Anodic Alumina Oxide (AAO) by One Step Anodization at low Voltage..Ph.D Thesis, Faculty of Engineering, Cairo University, Egypt (2013).

[82] Habazaki, H, Shimizu, K, Skeldon, P, Thompson, G. E, Wood, G. C, & Zhou, X. Nanoscale Enrichments of Substrate Elements in the Growth of Thin Oxide Films. Corrosion Science (1997). , 39, 731-737.

[83] Zaraska, L, Sulka, G. D, Szeremeta, J, & Jaskula, M. Porous Anodic Alumina Formed by Anodisation of Aluminium Alloy (AA1050) and High Purity Aluminium. Electrochimica Acta (2010). , 55, 4377-4386.

[84] Garcia-vergara, S. J, Iglesias-rubianes, L, Blanco-pinzon, C. E, Skeldon, P, Thompson, G. E, & Campestrini, P. Mechanical Instability and Pore Generation in Anodic Alumina. P. Roy Soc. Lond. A Mat. (2006). , 462, 2345-2358.

[85] Li, F, Zhang, L, & Metzger, R. M. On the Growth of Highly Ordered Pores in Anodized Aluminium Oxide. Chem. Mater. (1998). , 1998(10), 2470-2480.

[86] Diggle, J. W, Downie, T. C, & Goulding, C. W. Anodic Oxide Films on Aluminium. Chem. Review (1969). , 69, 365-405.

[87] Uchi, H, Kanno, T, & Alwitt, R. S. Structural Features of Crystalline Anodic Alumina Films. Journal of. Electron. Society (2001). 148, B17-B23.

[88] De Azevedo, W. M, De Carvalho, D. D, Khoury, H. J, & De Vasconcelos, E. A. Da Silva E.F. Jr. Spectroscopic. Characteristics of Doped Nanoporous Aluminium Oxide. Material Science Engineering B. (2004). , 112, 171-174.